BOSE CONDENSATION
IN A
MODEL MICROCAVITY

BOSE CONDENSATION

IN A

MODEL MICROCAVITY

Paul Roger Eastham

ROBINSON COLLEGE
UNIVERSITY OF CAMBRIDGE

TO CHARLIE AND MY PARENTS

Contents

Preface

This thesis describes work undertaken at the Cavendish Laboratory between October 1997 and November 2000, under the supervision of Professor Peter Littlewood.

Published Work

Some of the work reported in this dissertation has been published, or is in preparation for publication, in the papers

- "The thermal equilibrium of a pumped model microcavity, from polaritons to Bose condensation", in preparation for Physical Review B.

- "Bose condensation in a model microcavity", P. R. Eastham and P. B. Littlewood, Solid State Communications, 116 (2000) 357–361.

- "Exciton condensation", P. B. Littlewood and P. Eastham, in Proceedings of the NATO Advanced Research Workshop "Optical Properties of Semiconductor Nanostructures", NATO Sciences High Technology Series, Kluwer, 2000.

Declaration of Originality

This dissertation is the result of my own work and includes nothing with is the outcome of work done in collaboration. This dissertation has not been submitted, in whole or in part, for any degree or diploma other than that of Doctor of Philosophy at the University of Cambridge.

Paul Roger Eastham
Robinson College
November 2000

Summary

CAVITY POLARITONS are particles which are formed from photons confined to a cavity coupled to electronic excitations such as semiconductor excitons. Since the observation of cavity polaritons in 1992, there has been considerable interest in the quantum statistical behaviour of cavity polaritons. This thesis is a theoretical study of one of the most spectacular quantum statistical behaviours, Bose condensation, for cavity polaritons.

In this thesis, we investigate Bose condensation of cavity polaritons in a generic model of photons interacting with electronic excitations. The model we consider is a generalisation of the Dicke model, familiar from quantum optics. It consists of a single bosonic oscillator, describing the electromagnetic field in a cavity, interacting with a large number of two-state oscillators with a distribution of energies. These oscillators could represent, for example, excitons bound to traps in a disordered semiconductor.

Bose condensation is a phenomenon associated with conserved particles in thermal equilibrium. Thus to investigate Bose condensed polaritons we study the thermodynamics of the model at a fixed number of polaritons. We do this using two techniques: a variational approach, and a more powerful path-integral technique. The latter allows us to give an essentially exact description of both the thermodynamics and the excitations of the model.

Acknowledgments

BOSE CONDENSATION
IN A
MODEL MICROCAVITY

Chapter 1

INTRODUCTION

A POLARITON [1, 2] IS THE QUANTUM OF THE ELECTROMAGNETIC FIELD IN A DIELECTRIC. The behaviour of light in a dielectric is governed by the properties of polaritons, not the properties of photons. The textbook model of a dielectric as a set of classical harmonic oscillators displays much of the basic physics of polaritons. A plane wave eigenmode of the bare electromagnetic field induces an oscillating polarisation in the microscopic oscillators. If these oscillators are dense on the scale of the wavelength of light then the induced macroscopic polarisation will be a plane wave of the same wavevector and frequency as the driving field, which is therefore coupled to the original eigenmode of the field. Each eigenmode of this coupled system is a polariton: a mixture of a plane wave of the electromagnetic field and a plane wave polarisation.

1.1 EXCITONS

The polarisability of dielectrics can come from both the lattice and the electronic states, so we can have polaritons formed from photons coupled to phonons and from photons coupled to electronic excitations. The classic example of an isolated electronic excitation which can be directly coupled to light, and so forms polaritons, is an exciton in a direct-gap semiconductor [3].

The bandstructure of an idealised direct-gap semiconductor, shown in Fig. 1.1, consists of a completely filled valence band and a completely empty conduction band. The extrema of the conduction and valence bands are both at the centre of the Brillouin zone. It is possible for such a semiconductor to absorb a photon by transferring an
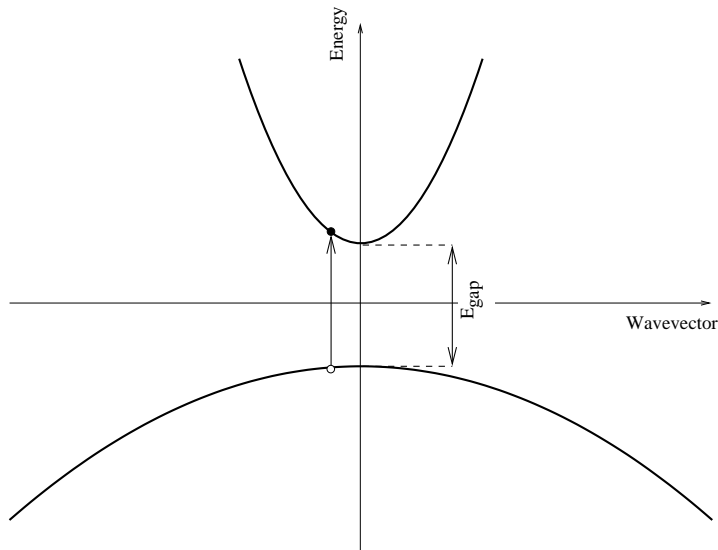
Figure 1.1: An idealised bandstructure for a direct-gap semiconductor, in the vicinity of the Fermi energy and the centre of the Brillouin zone, comprising a completely filled valence band and an empty conduction band. The arrow depicts an electronic excitation of such a semiconductor in the absence of electron-electron interactions, in which an electron is transferred from the valence to the conduction band, leaving a hole in the valence band.

electron from the valence band to the conduction band, so that a photon is converted into an electron-hole pair. Since an electron and a hole have opposite charges, such an electron-hole pair can lower its energy by using the Coulomb interaction to form a bound state known as an exciton. An exciton is the lowest energy excited state of a pure semiconductor.

It is customary to consider two limiting types of excitons, depending on their size: Frenkel excitons are tightly bound atomic scale objects, while Wannier excitons are weakly bound objects which extend over many lattice spacings. For the moment we consider the latter limit, which is realised in most of the common inorganic semiconductors.

2

Because a Wannier exciton extends over many lattice spacings, it can be described without reference to the microscopic structure of its constituent electronic states. It is sufficient to treat the electron and hole as particles propagating in free space, with the effects of the lattice on the motion of these particles taken into account by effective masses. Thus the singly excited states of the semiconductor, consisting of one electron and one hole, are described by an effective Hamiltonian

$$H = \frac{\boldsymbol{p}_e^2}{2m_e} + \frac{\boldsymbol{p}_h^2}{2m_h} - \frac{e^2}{4\pi\epsilon_r\epsilon_0|\boldsymbol{r}_e - \boldsymbol{r}_h|}, \tag{1.1}$$

where $\boldsymbol{r}_e$ and $\boldsymbol{r}_h$ are the positions of the electron and hole and $\boldsymbol{p}_e$ and $\boldsymbol{p}_h$ their momenta. We have assumed that the effective masses of the electron and the hole, m_e and m_h, are isotropic. The electron and the hole interact through the Coulomb interaction[1] in the dielectric background of the semiconductor; the relative permittivity ϵ_r of the semiconductor takes into account the screening of the interaction by the remaining valence electrons and the lattice.

The Hamiltonian (1.1) is analogous to that of the hydrogen atom, with the masses of the electron and proton replaced with effective masses, and the dielectric constant of the vacuum replaced with that of the semiconductor. Its eigenstates comprise a series of bound states, the excitons, and a continuum of ionized states describing unbound electrons and holes. Using $\boldsymbol{R}$ to denote the centre of mass coordinate and $\boldsymbol{r}$ the relative coordinate of the electron and hole, the bound states may be written as

$$F(\boldsymbol{R}, \boldsymbol{r}) = \frac{1}{\sqrt{V}}e^{i\boldsymbol{Q}.\boldsymbol{R}}\phi_n(\boldsymbol{r}). \tag{1.2}$$

The first term in the wavefunction (1.2) describes the free motion of the centre of mass of the exciton. The second is a hydrogen-like bound state in the relative motion, with principal quantum number

---

[1]While there is also an exchange interaction, it is small for Wannier excitons since the electron and hole are widely separated.

$n = 1, 2, 3 \ldots$. The binding energy is, in eV,

$$eE_b = \frac{e^2}{8\pi\epsilon_r\epsilon_0 a_0 n^2},$$

where the exciton Bohr radius is

$$a_0 = \frac{4\pi\epsilon_r\epsilon_0\hbar^2}{e^2\mu},$$

and μ is the reduced mass of the electron and hole. We see that for small effective masses and large dielectric constants the exciton is indeed weakly bound and large, so that the effective mass approximation is consistent. As an example, the relative permittivity of GaAs is ~ 10 while the ratio of the reduced mass to the bare electron mass is ~ 0.05. Thus the exciton Bohr radius is $\sim 100\text{Å}$ and the binding energy of the $n = 1$ state is $\sim 10\text{meV}$.

Excitons are neutral excitations with an inhomogeneous charge distribution: they are *quanta of the electronic polarisation* [1, 3, 4], which can couple to the transverse electromagnetic field. To describe the coupling between excitons and light, we need the actual electronic state corresponding to (1.2). This state can be compactly expressed using the formalism of second quantization, with the Bloch states

$$\psi_{\boldsymbol{k},l}(\boldsymbol{r}) = \frac{1}{\sqrt{V}}e^{i\boldsymbol{k}.\boldsymbol{r}}u_{\boldsymbol{k},l}(\boldsymbol{r}) \tag{1.3}$$

as a basis. These states are labelled by a wavevector in the first Brillouin zone, $\boldsymbol{k}$, and a band index l. V is a quantization volume. We use $c_{\boldsymbol{k}}^{\dagger}$ to denote the creation operator for an electron in the conduction band and $d_{\boldsymbol{k}}^{\dagger}$ the creation operator for a hole in the valence band. The electronic wavefunction for a semiconductor containing one exciton of wavevector $\boldsymbol{Q}$ is a superposition of free electron-hole pair states with wavevectors near to zero

$$|\boldsymbol{Q}, n\rangle = D_{\boldsymbol{Q},n}^{\dagger}|0\rangle = \frac{1}{\sqrt{V}}\sum_{\boldsymbol{k}}\phi_n(\boldsymbol{k})c_{\boldsymbol{k}+\frac{\boldsymbol{Q}}{2}}^{\dagger}d_{-\boldsymbol{k}+\frac{\boldsymbol{Q}}{2}}^{\dagger}|0\rangle. \tag{1.4}$$

For simplicity, we have taken the electron and hole effective masses to

4

be equal. $\phi_n(\boldsymbol{k})$ is the Fourier transform of the internal wavefunction of the exciton, $\phi_n(\boldsymbol{r})$, and $|0\rangle$ is the ground state of the semiconductor.

Equation (1.4) defines the exciton creation operator $D^\dagger_{\boldsymbol{Q},n}$. Since excitons are bound states of two fermions, they are bosons at low densities. This important property is reflected in the commutation relation for the exciton operators

$$
\begin{aligned}
[D_{\boldsymbol{Q}',n'}, D^\dagger_{\boldsymbol{Q},n}] &= \frac{\delta_{\boldsymbol{Q},\boldsymbol{Q}'}}{V} \sum_{\boldsymbol{k}} \phi^*_{n'}(\boldsymbol{k})\phi_n(\boldsymbol{k})\Big(1 - d^\dagger_{-\boldsymbol{k}+\frac{\boldsymbol{Q}}{2}} d_{-\boldsymbol{k}+\frac{\boldsymbol{Q}}{2}} \\
&\qquad\qquad - c^\dagger_{\boldsymbol{k}+\frac{\boldsymbol{Q}}{2}} c_{\boldsymbol{k}+\frac{\boldsymbol{Q}}{2}}\Big) \\
&= \delta_{\boldsymbol{Q},\boldsymbol{Q}'}\left[\delta_{n,n'} + \mathcal{O}(Na_0^3/V)\right],
\end{aligned}
\tag{1.5}
$$

where N/V is density of excitons.

1.1.1 The Exciton-Photon Interaction

In the Coulomb gauge, there is a linear coupling between the vector potential and the mechanical momentum of the electrons in the semiconductor

$$
H_{int} = -\frac{e}{m}\sum \boldsymbol{A}.\boldsymbol{p}_i,
\tag{1.6}
$$

where the sum is over all the electrons. Since we can decompose the electromagnetic field into plane waves, we begin by considering the coupling to a single plane wave of amplitude A_0 and polarisation $\boldsymbol{e}_\lambda$,

$$
\boldsymbol{A}_{\boldsymbol{K}}(\boldsymbol{r}) = A_0 \boldsymbol{e}_\lambda e^{i\boldsymbol{K}.\boldsymbol{r}}.
$$

This plane wave couples the conduction and valence bands to each other, as well as coupling the electrons within each band. The intra-band part of this coupling is irrelevant to the optics of excitons. The remaining inter-band part of (1.6) can be written as

$$
H_{int} = -A_0 \frac{e}{m} \sum_{\boldsymbol{k}} \left(c^\dagger_{\boldsymbol{K}+\boldsymbol{k}} d^\dagger_{-\boldsymbol{k}} g^{\boldsymbol{K}+\boldsymbol{k},\boldsymbol{k}}_{c,v} + d_{-\boldsymbol{K}-\boldsymbol{k}} c_{\boldsymbol{k}} g^{\boldsymbol{K}+\boldsymbol{k},\boldsymbol{k}}_{v,c} \right),
\tag{1.7}
$$

with a coupling strength determined by the polarisation of the field and the form of the Bloch functions

$$g_{l',l}^{k',k} = e_\lambda \cdot \frac{1}{\Omega} \int u_{k',l'}^* p u_{k,l} d^D r.$$

Here the integral is taken over a single unit cell of volume Ω. The matrix element of the coupling between the ground state and a single exciton state is

$$
\begin{aligned}
\langle Q, n | H_{int} | 0 \rangle &= -A_0 \frac{e}{m} \sum_{k,k'} \phi_n^*(k) \langle 0 | d_{-k+\frac{Q}{2}} c_{k+\frac{Q}{2}} c_{K+k'}^\dagger d_{-k'}^\dagger | 0 \rangle \\
&= -A_0 \frac{e}{m} \delta(K - Q) \sum_k \phi_n^*(k) g_{c,v}^{k+\frac{K}{2}, k-\frac{K}{2}} \\
&\approx -A_0 \frac{e}{m} \delta(K - Q) g_{c,v}^{0,0} \phi_n^*(0), \quad (1.8)
\end{aligned}
$$

where we have used the fact that the exciton is large in real space to approximate the inter-band matrix element g by its value at $k = 0$; this is the electric-dipole approximation. In this approximation, the matrix element for the creation of an exciton is proportional to $\phi_n(0)$, which is the probability amplitude that the electron and the hole are at the same point in space. Thus the s-wave excitons, for which $\phi_n(0) \neq 0$, are coupled to light provided the transition between the conduction and valence bands is dipole-allowed (i.e. $g_{c,v}^{0,0} \neq 0$).

An electromagnetic field of wavevector K couples both to the discrete set of exciton states and the continuum of unbound electron-hole pair states. If the electromagnetic field is weak only a small number of excitations will be involved, and so their interaction can be neglected. We can then write an effective Hamiltonian describing photons propagating in a semiconductor

$$H = H_{\text{field}} + H_{\text{e-ex}} + H_{\text{int}}, \quad (1.9)$$

where H_{field} describes the bare electromagnetic field, $H_{\text{e-ex}}$ the bare electronic excitations, and H_{int} the coupling between the electromagnetic field and the electronic excitations. Since this Hamiltonian is linear we will write only part of it, describing a single exciton transi-

tion and a single polarisation of the photons. The free part is

$$H_{\text{field}} + H_{\text{e-ex}} = \sum_{\boldsymbol{k}} E_\psi(\boldsymbol{k}) \psi_{\boldsymbol{k}}^\dagger \psi_{\boldsymbol{k}} + E_{ex}(\boldsymbol{k}) D_{\boldsymbol{k}}^\dagger D_{\boldsymbol{k}}, \qquad (1.10)$$

where ψ is the photon annihilation operator and D the exciton annihilation operator. The photons and excitons have the dispersion relations

$$
\begin{aligned}
E_\psi(\boldsymbol{k}) &= \hbar c |\boldsymbol{k}| \\
E_D(\boldsymbol{k}) &= E_0 + \frac{\hbar^2 |\boldsymbol{k}|^2}{2 m_{ex}}
\end{aligned}
$$

respectively, where $E_0 = E_{gap} - E_b$ is the rest energy of the exciton and $m_{ex} = m_e + m_h$ is the exciton mass. Combining the standard decomposition of the free electromagnetic field into plane wave eigenstates

$$\boldsymbol{A}(\boldsymbol{x}) = \sum_{\boldsymbol{k}} \sqrt{\frac{\hbar c \mu_0}{8 V |\boldsymbol{k}|}} \boldsymbol{e}_\lambda e^{i\boldsymbol{K} \cdot \boldsymbol{x}} (\psi_{\boldsymbol{k},\lambda} + \psi_{-\boldsymbol{k},\lambda}^\dagger),$$

with the matrix element (1.8) gives the interaction between excitons and photons

$$
\begin{aligned}
H_{int} &= -\frac{e}{m} \sum_{\boldsymbol{k}} \sqrt{\frac{\hbar c \mu_0}{8 V |\boldsymbol{k}|}} \left(\psi_{\boldsymbol{k}} + \psi_{-\boldsymbol{k}}^\dagger \right) \qquad (1.11) \\
&\quad \times \left(g_{v,c}^{0,0} \phi(0) D_{-\boldsymbol{k}} + g_{c,v}^{0,0} \phi^*(0) D_{\boldsymbol{k}}^\dagger \right).
\end{aligned}
$$

1.1.2 EXCITON POLARITONS

The Hamiltonian (1.9-1.11) is a microscopic version of the classical physics described at the beginning of this chapter: each plane wave photon is coupled to a plane wave polarisation which, at low densities where the excitons are bosons, has the dynamics of a harmonic oscillator. Let us demonstrate the formation of polaritons in this microscopic theory.

We simplify H_{int} by dropping the terms which describe the simul-

taneous creation or annihilation of a photon and an exciton,

$$\left(\psi_{\boldsymbol{k}} + \psi^{\dagger}_{-\boldsymbol{k}}\right)\left(D_{-\boldsymbol{k}} + D^{\dagger}_{\boldsymbol{k}}\right) \rightarrow D^{\dagger}_{\boldsymbol{k}}\psi_{\boldsymbol{k}} + \psi^{\dagger}_{-\boldsymbol{k}}D_{-\boldsymbol{k}},$$

which is known as the rotating-wave approximation [5]. It is justified close to resonance, where the terms retained describe the resonant coupling between the two oscillators, while those dropped describe non-resonant processes. We take the exciton-photon coupling strength to be real, and denote it by $g(|\boldsymbol{k}|)$. At low densities where the excitons are bosons, the Hamiltonian (1.9-1.11) in the rotating-wave approximation can be diagonalized by the unitary transformation

$$\begin{pmatrix} p_{\boldsymbol{k},1} \\ p_{\boldsymbol{k},2} \end{pmatrix} = \begin{pmatrix} \cos\theta_{\boldsymbol{k}} & -\sin\theta_{\boldsymbol{k}} \\ \sin\theta_{\boldsymbol{k}} & \cos\theta_{\boldsymbol{k}} \end{pmatrix} \begin{pmatrix} \psi_{\boldsymbol{k}} \\ D_{\boldsymbol{k}} \end{pmatrix},$$

from excitons and photons to two types of polariton, with annihilation operators p_1, p_2. The diagonalized Hamiltonian,

$$H = \sum_{\boldsymbol{k}} E_1(\boldsymbol{k})p^{\dagger}_{\boldsymbol{k},1}p_{\boldsymbol{k},1} + E_2(\boldsymbol{k})p^{\dagger}_{\boldsymbol{k},2}p_{\boldsymbol{k},2},$$

describes non-interacting polaritons which have the dispersion relations

$$E_{1,2}(\boldsymbol{k}) = \frac{1}{2}\left[E_{\psi}(\boldsymbol{k}) + E_D(\boldsymbol{k}) \pm \sqrt{(E_D(\boldsymbol{k}) - E_{\psi}(\boldsymbol{k}))^2 + 4g(|\boldsymbol{k}|)^2}\right].$$
$$(1.12)$$

The polariton dispersions and the mixing angle $\theta_{\boldsymbol{k}}$ are illustrated in Fig. 1.2[2]. Near to the resonance of the bare excitons and photons the polaritons are significantly different from excitons or photons, and the polariton dispersions show the level repulsion characteristic of coupled oscillators. This region is often referred to as the strong-coupling regime, because it cannot be described by perturbation theory in the

---

[2]This figure shows up a peculiar feature of the dispersion (1.12): at zero wavevector, the energy of the lower polariton lies below the energy of the vacuum. This implies that the conventional ground state of a dipole-active semiconductor is unstable, an incorrect result which is an artifact of the rotating wave approximation.
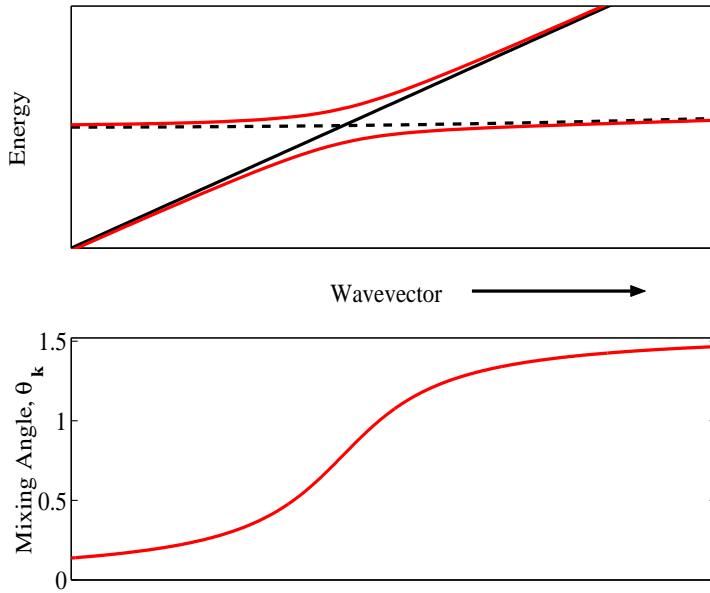
Figure 1.2: Illustration of the polariton (red), photon (solid black) and exciton (dashed black) dispersions in a bulk semiconductor, and the corresponding variation in the mixing angle $\theta_{\boldsymbol{k}}$ with wavevector.

coupling. This can be seen by noting that the polariton energies do not have a Taylor expansion in g when

$$|E_\psi(\boldsymbol{k}) - E_D(\boldsymbol{k})| < g.$$

1.2 CAVITY POLARITONS

In 1992, Weisbuch et al. [6] demonstrated the strong-coupling regime for excitons coupled to photons confined in a wavelength-sized cavity. Such a cavity is referred to as a *microcavity*; the mixed eigenstates of exciton and photons which form in the strong-coupling regime of microcavities [7] are known as *cavity polaritons*.

The system studied by Weisbuch et al., illustrated in the top part

9
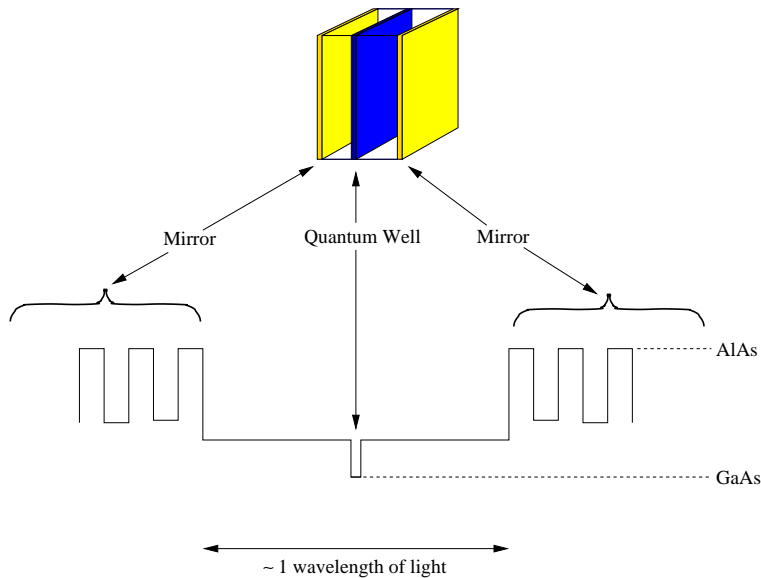
Figure 1.3: The experimental set up of Weisbuch et al., adapted from [6]. The upper part of the figure illustrates the basic structure of their planar microcavity, while the lower part shows the band-structure which actually forms this device. Only the beginning of the mirror stack is shown. The actual system contains several quantum wells at the centre of the cavity, rather than the single well illustrated here.

of Fig. 1.3, is essentially a Fabry-Pérot resonator containing a set of quantum wells. It is constructed from layers of (Ga,Al)As with various dopings, producing a bandstructure for the conduction band shown in the lower part of Fig. 1.3. The mirrors are distributed Bragg reflectors, which are interference devices constructed by using alternating layers of doping to produce alternating layers of high and low refractive index. Choosing the optical thickness of each layer to be $\lambda/4$ produces a mirror with a very high reflectivity over a broad range of wavelengths (a "stop-band") centred on λ.

Photons in such a planar cavity, with energies inside the stop-band of the mirrors, are quantized in the direction perpendicular to

the plane of the mirrors. They have allowed wavevectors

$$|k_z| = \frac{\pi m}{L} \qquad m = 1, 2, 3 \ldots,$$

where L is an effective separation for the mirrors which takes into account the finite penetration of the field into the mirrors [7]. There is no confinement parallel to the mirrors however, so that each of these confined modes is associated with a continuum of propagating modes with an in-plane dispersion

$$
\begin{aligned}
E_\psi(\boldsymbol{k}) &= \hbar c |\boldsymbol{k}| \\
&= \hbar c \sqrt{k_z^2 + |\boldsymbol{k}_\|^2} \\
&\approx \hbar c \left(|k_z| + \frac{|\boldsymbol{k}_\||^2}{2|k_z|} \right).
\end{aligned}
\tag{1.13}
$$

The low lying electron and hole states in the microcavity are confined in an analogous way by the quantum wells, so that lowest energy electronic excitations are two-dimensional excitons in each of the wells. Each two-dimensional exciton is formed from electron and hole states in the lowest subband of the quantum well. Such a two-dimensional exciton is more strongly bound than the three-dimensional exciton, with a binding energy increased by as much as a factor of four.

The size of the optical cavity is chosen so that photons with $\boldsymbol{k}_\| = 0$ and a small m, typically $m = 2$, are close to resonance with the quantum well exciton. The quantum wells are positioned at an antinode of the field for these photons, so that they are coupled to the excitons. In this configuration, photons with other values for k_z are far removed in energy and may be ignored.

The conventional picture [6] of these confined polaritons is similar to the microscopic theory of bulk polaritons discussed in subsection 1.1.2. The quantum well is assumed to be translationally invariant parallel to the plane of the mirrors, so that the excitons are propagating states with a well defined in-plane wavevector $\boldsymbol{k}_\|$. Momentum conservation in the plane then ensures that each of these exciton states is coupled only to a single mode of the electromagnetic field with the

11
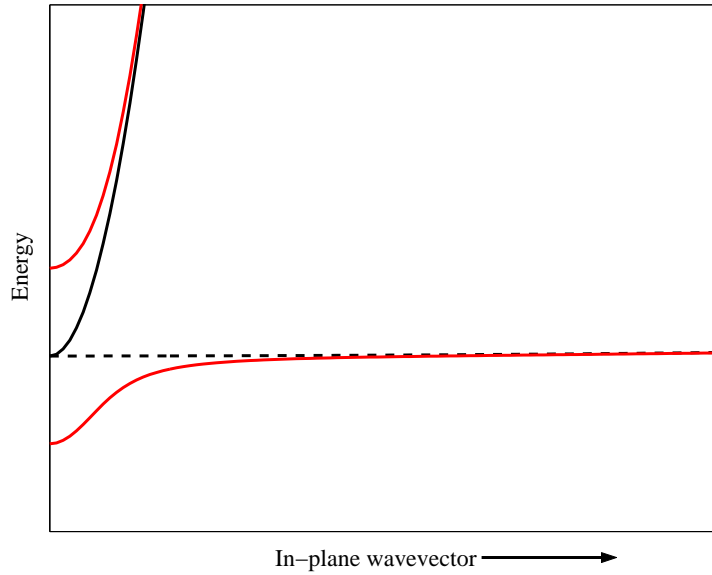
Figure 1.4: Illustration of the polariton (red), photon (solid black), and exciton (dashed black) dispersions for an ideal quantum well embedded in a planar microcavity. We have chosen k_z so that the excitons and photons are resonant at zero in-plane momentum.

same in-plane wavevector. Thus the form of the Hamiltonian is identical to (1.9-1.11), and the polariton energies are given by (1.12) with the two-dimensional photon dispersion (1.13). The resulting polariton energies are illustrated in Fig. 1.4.

Cavity polaritons are coupled to photons outside the cavity due to the finite mirror reflectivity. Because of this, they can be directly probed in properties such as the reflectivity or luminescence spectra of the cavity. While bulk polaritons can also be probed in this way, the interpretation of bulk measurements is complicated [2, 7] by two delicate issues: the photon-polariton coupling at the interface, and the transport of polaritons in the crystal. Understanding the coupling is difficult because the interface breaks momentum conservation, so that there can be polaritons with two different wavevectors inside the sample coupled to photons of a single wavevector outside. This does not

12

occur in the cavity system, because there is no longer a component of the wavevector perpendicular to the interface. Describing bulk luminescence requires a theory of transport because it is only at the surface of the sample that polaritons are coupled to photons; again, this issue does not arise for cavity polaritons, since there is no transport to the interfaces.

Another advantage of cavities over bulk systems for studying the strong-coupling regime is the ability to tune the energy of the photons through the energy of the excitons. This can be done either by varying the in-plane wavevector, i.e. making measurements at finite angles of incidence, or by varying the length of the cavity. The length of the cavity can be varied in a single experiment, by growing the cavity as a wedge shape and making measurements at different positions on the sample.

Cavity polaritons were first reported in the normal-incidence reflectivity spectra shown as Fig. 2 of Ref. [6]. The different curves correspond to different detunings between the bare exciton and photons, obtained by varying the size of the cavity as discussed above. In general, the reflectivity dips sharply at the energies of the two $\boldsymbol{k}_\parallel = 0$ polaritons, since it is only at these energies that the incident photons can be transferred across the cavity; the amplitude of these dips varies with the photon component of the polariton. Far from resonance one of the polaritons has almost no photon component, so only a single dip is visible on the top left curve. As the cavity is tuned towards resonance, both polariton branches acquire a significant photon component, so two dips can be seen in the reflectivity. The symmetrical curve occurs exactly at resonance, when the two polaritons are equal mixtures of exciton and photon. Because of the characteristic level repulsion of the strong-coupling regime, the polariton energies are different even when the exciton and photon are degenerate.

There is a great deal of physics in these systems beyond that in the two-dimensional analog of (1.9–1.11). An important issue is the presence of damping, and hence finite linewidths, for both the exciton and the photon. This is relevant because the strong-coupling regime only exists when two *sharp* resonances are coupled together. For the strong-coupling regime to exist for damped excitations, the linewidths

13

must be small compared with the coupling strength

$$\gamma \lesssim g. \tag{1.14}$$

This condition applied, for example, to the exciton linewidth means that the polarisation induced by the cavity field must remain long enough for the cavity field to respond to its creation. The requirement (1.14) prevents strong-coupling behaviour for an isolated, excited atom in free space since, as there is no momentum conservation, the atom couples to a continuum of photon modes. The formation of mixed modes is then replaced with irreversible decay of the atom as the excitation is transferred into the continuum.

The cavity modes are damped by the escape of photons. The confined mode, $\boldsymbol{k}_\parallel = 0$, only decays because of the finite reflectivity of the mirrors. It typically has a lifetime of a few picoseconds, corresponding to linewidths of the order 0.1–1 meV. At a simple level, we can include this linewidth as an imaginary part in the photon energy. In Fig. 1.5, we plot the polariton energies (1.12) as a function of the imaginary part of the photon energy, when the exciton and photon are resonant and the exciton is undamped. Note the reduction and eventual disappearance of the level repulsion, characteristic of the strong-coupling regime, as the damping increases.

The broadening of the exciton and the destruction of the strong coupling behaviour is connected to another important issue in these systems: nonlinearity [8, 9]. So far we have assumed that the excitation of the quantum well is negligible, so that the interaction between excitations can be neglected. Such a theory describes the linear optical properties of the microcavity. If we probe the cavity using stronger fields, we will create a finite density of excitons and unbound electron-hole pairs in the quantum wells. If this density is not too high excitons continue to exist, although they may be shifted in energy and acquire a lifetime as a result of the interactions. The coupling between excitons and photons can also be reduced, for two main reasons: (1)At finite densities, the exclusion principle blocks the creation of an exciton from a photon. The electron-hole pair states which are already occupied are not available for the formation of further excitons. This nonlinearity is known as "phase space filling". (2)The Coulomb inter-

14
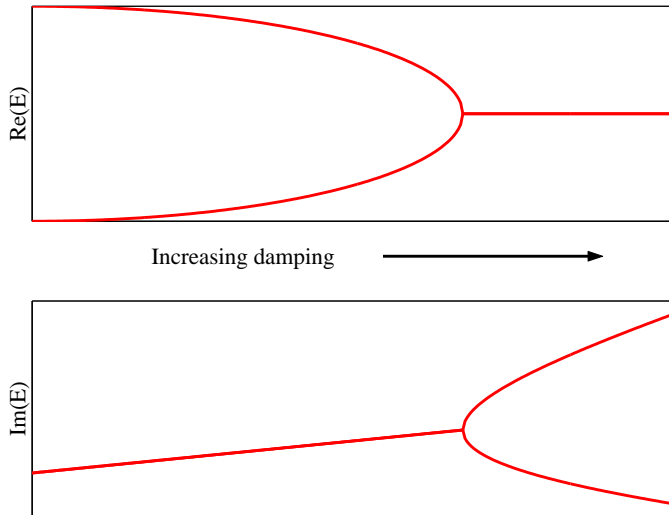
Figure 1.5: Crossover from strong to weak coupling with increasing damping of the photon. The upper and lower panels are the real and imaginary parts of the energies (1.12) of the coupled modes, as a function of the imaginary part of the photon energy. We have taken the exciton and photon to be resonant, so that $\Re E_\psi = \Re E_D$.

action between the electron and hole in the exciton can be screened by the other excitations. Thus the exciton will be larger, and hence more weakly coupled to light. With increasing density, this screening process eventually completely destroys the excitons. Since increasing excitation can increase the exciton linewidth and decrease the exciton-photon coupling, increasing density eventually violates the inequality (1.14) and destroys the strong-coupling regime. While this has been demonstrated experimentally [10, 11], there is no consensus concerning the importance of the different nonlinearities to the destruction of the strong-coupling regime.

Since these pioneering experiments using GaAs quantum well excitons in planar optical cavities, there have been several other realisations of cavity exciton-polaritons, using different geometries and approaches to photon confinement, or different materials containing

excitons. Polaritons have been realised in photon wires [12] and in pillar microcavities [13, 14]. Alternative dielectrics which have been used in planar optical cavities include films of organic semiconductor [15, 16], bulk GaAs [17], and (Zn, Cd)Se quantum wells [18].

These more recent realisations of cavity polaritons show up a flaw in the conventional picture discussed above. This picture is based on a perfect, infinite quantum well, where the bare electronic excitations are propagating states with a well defined momentum. Thus microscopic momentum conservation ensures that each exciton is coupled only to a single cavity mode, so that the condition (1.14) can be obeyed despite the presence of a continuum of cavity modes with different $k_\parallel$. Yet the real systems in which polaritons are observed contain structural disorder, and all bar one are two-dimensional. In these two-dimensional disordered systems, the excitons are localised rather than propagating states. If the localisation length is long compared with the wavelength of light, one could believe a picture based on microscopic momentum conservation. However, given the long wavelength of light, this is unlikely to be true in any of these systems. The problem is particularly clear for organic semiconductors, which are often highly disordered at the molecular level.

Structural disorder in quantum well systems [19–22] has a variety of origins. For example, one source of disorder is fluctuations of the alloying concentration across the sample; another is that the interfaces of the quantum well are not perfectly flat. It is generally assumed that this disorder is weak compared with the binding energy of the exciton, so that it may be treated as a potential acting on the centre of mass of the exciton. Thus the quantum well contains a set of exciton states with localised centre of mass wavefunctions. The energy distribution of these localised states corresponds to an *inhomogeneous linewidth* for the exciton, which is typically a few meV. This is actually the dominant broadening mechanism for quantum well excitons at low densities, far more important than any actual damping of the exciton. The correlation length of the disorder potential, and hence the spatial extent of the exciton, depends on the growth conditions of the sample [23]. In GaAs, this correlation length seems to vary between a few times the exciton Bohr radius and about ten times the exciton Bohr

16

radius [24].

There are two reasons why strong-coupling behaviour can be realised using localised excitations for which there is no microscopic momentum conservation, despite the condition (1.14). The first reason, which was mentioned at the beginning of this chapter, applies when there are many microscopic excitations in one wavelength of light. The excitations which couple to light are then coherent superpositions of many microscopic excitations. So long as the microscopic excitations remain mutually coherent, i.e. so long as the homogeneous linewidth of the excitations is small, this collective state couples only to one field mode. Interference of the microscopic polarisations effectively restores macroscopic momentum conservation. This is why strong-coupling behaviour shows up in the refractive index of sodium vapour [2]. The second reason is that optical cavities can produce sharp resonances in the photon density of states[3], so momentum conservation may not be required at any level. This is why strong-coupling behaviour has been observed for a few hundred sodium atoms in an optical cavity [25].

These considerations suggest that the conventional model of cavity polaritons, based on microscopic momentum conservation, is inappropriate in many experiments, and that a more appropriate model is a single mode of the electromagnetic field coupled to many microscopic excitations. In this thesis we will study one such model, a generalisation of the Dicke model [26, 27].

1.3   THE DICKE MODEL

The Dicke model, which is one of the basic models of quantum optics, was originally introduced to study the radiative decay of a gas. It treats each molecule in the gas as a two-state oscillator, corresponding to two possible electronic states of the molecule. The transition

---

[3]This depends on the cavity structure: the density of photon states in three-dimensional cavities would be completely discrete, but in an idealised planar cavity it would be the usual two-dimensional stepped density of states. In fact, it seems likely that the photon density of states in a real planar cavity has peaks at the energies of the $k_\parallel = 0$ modes, since these are only damped by the escape of photons through the mirrors, while the propagating modes can escape through the sides of the cavity.

17

between these two states occurs through the electric-dipole interaction with a single mode of the electromagnetic field. All other degrees of freedom of the molecules, including their dispersion, are neglected, as are any direct interactions between molecules.

As Dicke noted, a two-state oscillator is equivalent to a spin of magnitude one-half. Thus we can write the Hamiltonian of the Dicke model in a spin notation. The two eigenstates of σ_n^z, with eigenvalues $\pm\frac{1}{2}$, correspond to the two electronic states of the nth molecule. Using E_g to denote the energy separation of these eigenstates, g the strength of the electric-dipole transition between them, and ω_c the energy of the photon, we write the Hamiltonian of the Dicke model as

$$H = \omega_c \psi^\dagger \psi + \sum \left[E_g \sigma_n^z + g \left(\sigma_n^+ \psi + \psi^\dagger \sigma_n^- \right) \right], \qquad (1.15)$$

where the summations are over the N different molecules. We have made the rotating wave approximation, as on page 8. For simplicity, we have also assumed that the amplitude of the field mode at each molecule is the same for all the molecules, so that the coupling strength g does not depend on the index n.

There is an upper bound on the excitation of the molecules in the Dicke model, because the exclusion principle for the electrons prevents more than a single excitation existing on any one molecule. This *saturation nonlinearity* does not appear directly in the Hamiltonian (1.15), but is concealed in the commutation relations of the spin operators. While much of the present thesis concerns this nonlinearity, it is irrelevant for weak excitation. The model (1.15) then contains essentially the same physics as our earlier bosonic Hamiltonian (1.9-1.11).

Let us define, following Dicke [26], the total pseudospin operator $\boldsymbol{S}$ for the two level oscillators. The components of this spin are related in the obvious way to the components of the constituent spins $S^{x,y,z} = \sum \sigma_n^{x,y,z}$. Physically, S^z measures the total excitation, and S^+ the total dipole moment, of the gas. Note that the squared magnitude of the pseudospin, $\boldsymbol{S}^2$, with eigenvalues $S(S+1)$, is a conserved quantity.

The equivalence between the Dicke model and our earlier bosonic Hamiltonian exists because the photon is coupled to collective excitations of the gas. These excitations are created and annihilated by the

18

operators $S^{\pm}$. When the number of excited molecules $N_{ex} = S^z + N/2$ is small compared with the total number of molecules N, the commutation relation for these operators is a large number with a small operator part:

$$
\begin{aligned}
[S^-, S^+] &= -2S^z \\
&= N - 2N_{ex} \\
&\sim N.
\end{aligned}
\qquad (1.16)
$$

Thus, apart from a normalisation, the operators $S^{\pm}$ obey a bosonic commutation rule in the low excitation limit.

We can formalise this equivalence using the Holstein-Primakoff representation [28] for the spin operator $\boldsymbol{S}$. This transformation allows us to linearise the spin model (1.15) around the unexcited state, which is the state with

$$
\begin{aligned}
S^z|0\rangle &= -\frac{N}{2}|0\rangle \\
\boldsymbol{S}^2|0\rangle &= \frac{N}{2}\left(\frac{N}{2}+1\right)|0\rangle.
\end{aligned}
$$

The appropriate transformation, which expresses the operators for a spin of magnitude S in terms of a bosonic annihilation operator D, is

$$
\begin{aligned}
S^+ &= D^{\dagger}\left(\sqrt{2S - D^{\dagger}D}\right) \\
S^- &= \left(\sqrt{2S - D^{\dagger}D}\right)D \\
S^z &= D^{\dagger}D - S.
\end{aligned}
\qquad (1.17)
$$

In this representation, the ground state $|0\rangle$ is the vacuum state of these new bosons, and $D^{\dagger}D$ is the number of excited molecules. For weak excitation we may retain only the leading terms in the expansion of the square roots in (1.17). Inserting these leading terms into the Hamiltonian (1.15) recovers a bosonic model of the form (1.9-1.11). Note that while we could perform this procedure at finite excitations, the result would be a model of interacting bosons. The difference, (1.16), between the operators $S^{\pm}$ and the bosonic creation and annihilation

19

operators corresponds to interactions between the excitations.

1.4 Polaritons in Disordered Systems

We can generalise (1.15) to describe cavity polaritons in disordered electronic systems. Provided the electronic excitations are small compared with the wavelength of light, we can treat them as point-like objects just like the molecular excitations discussed by Dicke. Each two-level oscillator then corresponds to the presence or absence of a particular localised excitation. For example, in a quantum well each oscillator is associated with a particular eigenstate of the disorder potential, labelled by the variable n. The interaction between different excitations is irrelevant to the description of the weakly excited states of the system, so can be ignored just as in (1.15). The restriction to single occupancy may or may not be physical, but since it is irrelevant to the weakly excited states we may retain it. The only generalisation we must make is to allow the energy of the two level oscillators, and possibly the coupling strength, to vary between excitations. Thus we allow E_g and g to depend on n. We change notation slightly by expressing each two level oscillator in terms of two fermions with annihilation operators a and b, subject to the constraint

$$a^\dagger a + b^\dagger b = 1. \tag{1.18}$$

The Hamiltonian describing cavity polaritons for localised excitations is then

$$
\begin{aligned}
H &= \sum \frac{E_g(n)}{2}\left(b^\dagger b - a^\dagger a\right) + \omega_c \psi^\dagger \psi + H', \tag{1.19}\\
H' &= \frac{1}{\sqrt{N}} \sum \left(b^\dagger a \psi + \psi^\dagger a^\dagger b\right).
\end{aligned}
$$

Note that we have redefined the coupling constants by substituting $g \to g/\sqrt{N}$. This redefinition is necessary for the limit of many electronic states in the cavity, $N \to \infty$, to be well defined.

The model (1.19) was used to investigate polaritons in a disordered system by Houdré et al. [29]. The central results of their paper are that (1) an inhomogeneous linewidth has the same effect on the level

splitting as a homogeneous linewidth (see the top panel of Fig. 1.5), and (2) an inhomogeneous linewidth does not, in general, produce a linewidth for the polaritons (unlike the bottom panel of Fig. 1.5). Both of these can be understood on physical grounds. Recall that a driven oscillator radiates at its driving frequency, with an amplitude determined by how far off resonance it is driven. Thus an inhomogeneous broadening decreases the amplitude of the macroscopic polarisation induced by the cavity mode in the microscopic oscillators, as the oscillators move out of resonance, but does not produce any linewidth for this polarisation. Hence the polariton splitting is reduced by the inhomogeneous broadening, but not, in general, broadened.

When the electronic system is not completely homogeneous on the scale of the wavelength of light we expect some weak scattering of the photon into other wavevectors. Therefore, when the correlation length of the disorder is a finite fraction of the wavelength of light, we would expect some contribution to the polariton linewidth beyond that predicted by models like (1.19). However, even in the best quantum wells, where the correlation length might be as high as a tenth of the wavelength of the photon, this contribution is insignificant: treating the quantum well as macroscopically homogeneous gives a good account of the experimental linewidths [30, 31]. This is hardly surprising, since the radiative lifetime of a single localised exciton in a GaAs quantum well is thought to be around 100ps [32], which corresponds to an insignificant linewidth on the scale of the observed level repulsions.

1.5 Interactions and Localised Excitations

We have already mentioned some of the nonlinearities for quantum well excitons. Although the dominant nonlinearities in quantum wells have a common origin in the fermionic structure of the excitons, a complete theory of these nonlinearities is extremely difficult. In general, this difficulty is compounded by the presence of disorder. However, for some of the excitations in a disordered quantum well, and for the excitations in many other dielectrics, the nonlinearities are much simpler. These *localised, physically separated, saturable* excitations are

described by straightforward generalisations of the model (1.19), even at finite densities.

The most straightforward examples of such excitations are Frenkel excitons bound on impurities, and molecular excitons in organics. These are essentially electronic transitions between states of an impurity or of a molecule. The classic example of the former is the lasing transition in ruby [33], which is between the electronic states of the Chromium impurities. So long as the overlap between the orbitals of different impurities or molecules is small we can neglect the interaction between excitations on different sites. In general there will be several orbitals on each site, as well as a spin degeneracy, and possibly some interaction between excitations on the same site. The result of this will be a model which, like (1.19), comprises a set of sites, each of which can contain some small number of excitations, with no interaction between different sites.

A more subtle example is the low energy electronic excitations in a disordered quantum well. In general, these are excitons bound to traps in the disorder potential. The size of these traps is, at most, the correlation length of the disorder potential, which is typically a few times the exciton Bohr radius. Because of the fermionic structure of the excitons, each of these traps can contain only a few low-energy excitons.

A rather special example of excitons bound to traps in a disorder potential is provided by narrow ($\sim 30\text{Å}$) GaAs quantum wells. In such narrow wells, fluctuations in the thickness of the quantum well are a significant source of disorder. These fluctuations have a natural minimum amplitude corresponding to a single atom step in one of the interfaces. This can actually split the exciton luminescence line into two parts, with the lower line produced by excitons bound in rare traps formed from monolayer fluctuations in the well thickness [19], as illustrated in Fig. 1.6.

1.6 Quantum Statistical Effects in Cavities

The term *quantum statistics* refers to the quantum mechanical treatment of indistinguishable particles. Since cavity polaritons are in-
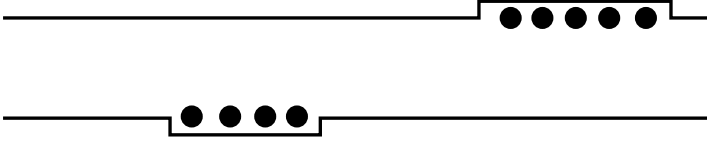
Figure 1.6: Illustration of low-energy excitons in a narrow quantum well. These quantum wells are believed to contain island-like structures produced by monolayer fluctuations in the thickness of the well. The figure shows a cross section of a well contaning such structures. The low energy excitons sit on these islands, producing a separate luminescence line which is split off from the luminescence line produced by excitons in the narrow part of the well.

distinguishable from one another, and may be considered as quantum mechanical particles, they should display effects due to quantum statistics.

Since cavity polaritons are photons coupled to other excitations, they are bosons. The most basic quantum statistical effect for bosons is stimulated scattering. According to the Fermi golden rule, the rate of some transition is proportional to the squared matrix element of the perturbation between the initial and final states. Thus a transition which involves adding a boson to a single particle eigenstate, with occupation N, occurs at a rate proportional to $N + 1$: the scattering into an eigenstate is stimulated (i.e. enhanced) by the particles already in that eigenstate. For photons this stimulation process is responsible for lasing.

There have been many experiments attempting to observe stimulated scattering for cavity polaritons. These experiments have focussed on the original system of a planar microcavity containing GaAs quantum wells, although II-VI quantum wells and bulk GaAs have also been used. In one type of experiment [34–36], a cavity is excited at energies above the energy of the low-wavevector polaritons. This highly excited cavity relaxes, leading to some population of the low-energy polaritons. This population is then observed as luminescence. For a weakly excited system, the relaxation is very inefficient, and the intensity of the luminescence at the energy of the $\boldsymbol{k}_{\parallel} = 0$ polariton is

rather small. Most of the excitation escapes from the cavity before reaching these low energies. However, there is a threshold excitation at which this luminescence becomes much more intense. This threshold behaviour is interpreted as stimulated scattering enhancing the relaxation towards the low energy polaritons.

A much cleaner approach to observing stimulated scattering involves directly creating a large population of polaritons at a single in-plane wavevector. This is done by exciting the cavity at a certain angle with a laser tuned to the corresponding polariton energy. In the presence of this population, a large gain is observed for a weak probe beam at another wavevector [37]. This gain is interpreted as stimulated scattering of the pump polaritons by the probe polaritons. More recently, similar effects have been reported in the absence of a probe beam [38].

These experiments, as well as lasers, involve stimulated scattering *far* from thermal equilibrium. *In* thermal equilibrium, stimulated scattering produces the Bose-Einstein distribution, and is partly responsible for the celebrated phenomenon of Bose-Einstein condensation. Thus the existence of stimulated scattering for polaritons suggests the possibility of a Bose-Einstein condensate of polaritons.

1.7 Bose-Einstein Condensation

A Bose-Einstein condensate [39] is a state of matter formed when a liquid or gas of bosons is cooled below a certain critical temperature. The classic example of Bose condensation is liquid Helium-4, which becomes a Bose condensate at about 2K. It is the formation of a Bose condensate in this liquid which is responsible for its celebrated superfluidity property. A less obvious example is the superconducting transition in conventional superconductors. Once again, the superflow property in these materials is the result of Bose condensation. For many years these two examples, along with Helium-3, have provided the only realisations of Bose condensates. In the last few years a new class of examples has been added to this short list by the realisation of Bose condensation in atomic vapours.

Bose condensation is the result of the quantum mechanical treat-

ment of identical particles. This is important for point-like bosons with energy E when the spacing between particles is comparable to the de Broglie wavelength $\lambda_B \sim \hbar/\sqrt{mE}$. We can estimate the critical temperature for a transition from a liquid or gas of point-like bosons to a Bose condensate by equating the separation between particles at a density ρ to the de Broglie wavelength at an energy kT. In three dimensions this gives

$$T \sim \frac{\hbar^2 \rho^{\frac{2}{3}}}{mk_B}, \tag{1.20}$$

Bose condensates of point-like bosons are so scarce because most Bose liquids solidify long before the temperature (1.20) is reached. Only Helium, with its small mass, remains a liquid.

There are three essential properties of real Bose condensates : (1) a macroscopic occupation of one of the single-particle eigenstates, (2) macroscopic phase coherence, and (3) broken gauge symmetry. The first property marks Bose condensation as a separate state of matter, since in the familiar states of matter the occupation of any single-particle eigenstate is negligible compared with the total number of particles. In an extended, homogeneous system, macroscopic occupation of a single-particle eigenstate implies that there are long range correlations in the phase of the boson field $\psi(\boldsymbol{r})$. This is the second property of *phase coherence*, meaning that the wavefunction of the macroscopically occupied state remains coherent over long distances. It is implied by the third property of *broken gauge symmetry*, which means that the local phase of the macroscopically occupied wavefunction acquires a well-defined value. In the absence of symmetry breaking, the number of particles in the macroscopically occupied eigenstate would suffice as an order parameter for Bose condensation. Broken gauge symmetry adds another component to this order parameter, which is the local phase of the macroscopically occupied eigenstate. The overall order parameter of the condensate is then the expectation value of the annihilation operator $\langle \psi(\boldsymbol{r}) \rangle$.

The broken gauge symmetry of a condensate is often compared to the broken rotational symmetry in a ferromagnet [40]. Even though the quantum mechanics of a magnet does not depend on its orientation, the direction of the magnetisation has a well-defined direction in

25

the ferromagnetic state. Analogously: even though quantum mechanics is independent of the phase of the wavefunction, for most purposes a Bose condensate is a state in which this phase adopts a well-defined value. This analogy assuages one difficulty with broken gauge symmetry: the prejudice that the phase of the wavefunction is not a physical quantity. It can be a physically meaningful quantity for certain classes of states in the limit of large numbers of particles. The same difficulty occurs in the magnetic case, since the direction of a microscopic angular momentum is not a physical quantity. But we have no problem with the direction of a macroscopic angular momentum.

Unfortunately, the standard textbook discussion of Bose condensation is in terms of a non-interacting Bose gas, and this model does not convincingly display any of the properties of real Bose condensates discussed above. However, we can introduce interactions which are so weak that they are irrelevant above the transition temperature, but generate the three properties discussed above below it. This is the weakly interacting Bose gas model studied by Bogolubov and others, which was instrumental in developing the concepts of Bose condensation.

Since weak interactions have little effect in the normal state, the instability of this state in the non-interacting gas remains instructive. The single particle eigenstates in a non-interacting Bose gas have energies

$$E_{\boldsymbol{k}} = \frac{\hbar^2 \boldsymbol{k}^2}{2m}.$$

Adopting the usual periodic boundary conditions on a cube of side L restricts the wavevector $\boldsymbol{k}$ to lie on a cubic lattice of lattice constant π/L. The occupation of a single eigenstate with energy $E_{\boldsymbol{k}}$ is given by the Bose function

$$n_{\boldsymbol{k}} = \frac{1}{e^{\beta(E_{\boldsymbol{k}} - \mu)} - 1}.$$

Notice the singularity in the ground state occupation as $\mu \to 0$. In three dimensions this singularity acquires a physical significance, because the chemical potential can be driven to zero by cooling the gas or increasing its density. To see this, note that the number of particles

26

in the gas is given by the sum over states of the occupation numbers,

$$N = \sum_{\boldsymbol{k}} n_{\boldsymbol{k}}. \tag{1.21}$$

Assume for a moment that $\mu < 0$. Then the variation in $n_{\boldsymbol{k}}$ between adjacent terms in the sum (1.21) is negligible in the thermodynamic limit $L \to \infty$. The sum may then be replaced by an integral in the usual way, giving for the density of the gas

$$\frac{N}{L^3} = \frac{1}{(2\pi)^3} \int \frac{1}{e^{\beta(E_{\boldsymbol{k}} - \mu)} - 1} d\boldsymbol{k}. \tag{1.22}$$

But for $\mu < 0$, the density (1.22) has an upper bound ρ_c in three dimensions. Above this critical density the assumption that $\mu < 0$ breaks down.

This critical density is the point where the normal Bose gas becomes unstable. Above the critical density the distribution function $n_{\boldsymbol{k}}$ must vary quickly on the scale of the spacing between the levels, so that the transition from the sum, (1.21), to the integral, (1.22), is not valid. To construct such a distribution we must place a macroscopic number of particles in a non-macroscopic number of states near to the ground state. We could place all the excess density $\rho - \rho_c$ into the ground state, so that the putative condensate would have at least the first two properties discussed above. However, there seems to be no clear reason [41] why all the excess particles should occupy just one of the single-particle states in this way.

This ambiguity is resolved by interactions [41, 42]. Because the singular states contain a macroscopic number of particles in a negligible energy range, an arbitrarily weak interaction can create a macroscopic energy difference between different singular states. In a simple Bose gas the interaction must be repulsive to prevent the gas collapsing to infinite density. Repulsive interactions select the singular distribution in which only a single quantum state is macroscopically occupied and push the other possibilities to macroscopically large energies. Attractive interactions, stabilised for example by a finite angular momentum, could select a different state [43].

Weak interactions also produce broken gauge symmetry [41, 42]. In the non-interacting model the ground state is a number state in the lowest single-particle eigenstate

$$(\psi^\dagger)^N |0\rangle. \tag{1.23}$$

With weak interactions, the part of the ground state wavefunction describing the occupation of this single-particle eigenstate is not a number state like (1.23), but a coherent state

$$e^{\phi \psi^\dagger} |0\rangle. \tag{1.24}$$

Here ϕ is the expectation value $\langle \psi \rangle$, which is the order parameter for the condensate. The basic reason why (1.24) is energetically favoured is that a finite interaction term mixes coherent states in the other single-particle levels into the coherent ground state (1.24). This leads to interference terms which can lower the interaction energy below that in a number state like (1.23). Furthermore, these interference terms lock the relative phases of all the single particle levels together. Once the coherent state is formed with a particular phase, it requires a finite energy to change the phase of one of the single particle states, and the gauge symmetry is broken.

While the weakly interacting Bose gas was instrumental in developing the concepts of Bose condensation, it has only found direct application with the realisation of atomic condensates. The interactions in superfluid Helium are far too strong to be treated by this theory, while in superconductors the internal structure of the particles which condense cannot be neglected.

None of the Bose condensates of condensed matter physics are formed from structureless bosons, but from bound states of an even number of fermions. If the density is sufficiently low that the spatial separation of such bound states is much greater than their size, and the temperature is low compared with their binding energy, the internal structure of the bound states may be ignored. They may be treated as simple, point-like bosons, as shown explicitly for excitons at zero temperature by the commutation relation (1.5).

The condensate in superconductors is formed from weakly-bound,

28

overlapping pairs of electrons known as Cooper pairs. These pairs cannot be treated as structureless bosons, and so cannot be described by the weakly-interacting Bose gas model. Nonetheless, they form a state which displays all the essential properties of a Bose condensate. But we must emphasise one important difference: while the transition in a weakly interacting Bose gas is associated with the centre of mass degree of freedom of the bosons, in the superconductor it is associated with the internal degrees of freedom of the pairs.

1.8 Bose Condensation of Cavity Polaritons

In this thesis, we will consider Bose condensation of cavity polaritons in the idealised model (1.19) of localised, physically separated, saturable excitations. Since Bose condensation is a thermal equilibrium phenomenon associated with conserved particles, we will consider the thermal equilibrium of the model (1.19) at a fixed number of polaritons. Physically, this corresponds to a situation in which polariton decay, arising from decay of the cavity mode and coupling of the electronic excitations to modes other than the cavity mode, is slow compared with the time required to reach thermal equilibrium at a fixed polariton number.

Before we can begin to explore polariton condensation, we must tackle the following inconsistency: Bose condensation is produced by interactions, while polaritons are linear response excitations. To overcome this inconsistency, we generalise the concept of a polariton to be the quantum of excitation of the coupled matter-light system. The polariton number is then the total number of photons and electronic excitations in the system. It is given by

$$N_{\mathrm{pol}} = L + N/2,$$

where L is the operator

$$L = \psi^\dagger \psi + \frac{1}{2} \sum b^\dagger b - a^\dagger a.$$

L is a conserved quantity for the model (1.19).

We must also revisit our assumption that there is only a single

relevant mode of the electromagnetic field in the cavity. When considering the linear-response dynamics of a cavity we gave two reasons for this (page 17): interference effects, and the selection of field modes by a cavity. When considering thermodynamics, we cannot apply the argument based on interference effects, since as the microscopic excitations thermalise their relative phases will be destroyed. However the second argument, based on the selection of field modes by a cavity, continues to apply.

For simplicity, we will take the coupling strengths $g(n)$ in (1.19) to be constant, $g(n) = g$. The expressions which we will derive may be generalised in the obvious way to allow for a distribution of these coupling strengths. To illustrate our results, we will take the energies of the two-level oscillators either to be uniform, or to have a Gaussian distribution centred on an energy E_0 with variance σg.

The thermal equilibrium of the Dicke model, (1.15), in the absence of an externally created population of polaritons, has been studied extensively since the pioneering exact solution of Hepp and Lieb [44]. These authors showed that, even in the absence of external excitation, the Dicke model has a phase transition to a Bose condensed state. This equilibrium condensate is a static, coherent state of photons: it is a ferroelectric [45]. The polariton condensate explored in the present thesis is an oscillating, quasi-equilibrium generalisation of this ferroelectric state.

In the next Chapter, we use a variational approach to find the ground state of the model (1.19) at fixed excitation L. In Chapter 3, we show that such a variational approach actually gives an exact description of the ground state at fixed excitation. We also consider finite temperatures, and construct a phase diagram. In Chapter 4, we use the expressions derived in Chapter 3 to study the excitations of the quasi-equilibrium states of the model (1.19). Finally, in Chapter 5 we summarise the conclusions and implications of our work, and suggest some problems for future study.

Chapter 2

THE GROUND STATE

T O BEGIN OUR INVESTIGATION OF POLARITON CONDENSATION, we use a variational approach to investigate the ground state of the model (1.19) at fixed excitation number L. Our variational wavefunction describes a Bose condensate of polaritons beyond the low-density regime in which polaritons are conventionally understood.

2.1 A VARIATIONAL WAVEFUNCTION

We must first guess a form for the variational wavefunction. To do this, recall that in section 1.3 we argued that in the limit of weak excitations the Dicke model is equivalent to a model of weakly-interacting, bosonic polaritons. In this limit the ground state must be a coherent state of polaritons. Beyond this limit we have generalised the concept of a polariton to be an excitation of the coupled system, counted by L. In general, such an excitation will be a superposition of an excitation of the cavity mode and an electronic excitation. This suggests that we try the variational wavefunction

$$|\lambda, w\rangle = e^{\lambda \psi^\dagger + \frac{1}{\sqrt{N}} \sum_n w_n b^\dagger a} |vac\rangle, \qquad (2.1)$$

where λ and the w_n are variational parameters, and $|vac\rangle$ is the state which has a single fermion in the lower state of each two-level oscillator.

The variational parameters w_n are the wavefunction for a collective excitation of the electronic states. While in the Dicke model, where the electronic excitations are all equivalent, this wavefunction must be a constant, the distribution of energies in the model (1.19) could produce non-trivial wavefunctions.

The electronic part of the variational wavefunction (2.1) is of the same form as the BCS wavefunction for a superconductor. This can be seen by expanding the part of the exponential which involves the fermionic operators. In this way we rewrite (2.1) as a superposition of a coherent state of the photons and a BCS state of the fermions

$$|\lambda, u, v\rangle = e^{\lambda \psi^\dagger} \prod_n (v_n b^\dagger + u_n e^{i\phi_n} a^\dagger)|0\rangle. \qquad (2.2)$$

Here λ, u_n, v_n, and ϕ_n are the variational parameters, and $|0\rangle$ denotes the vacuum state with no fermions in any of the levels. By construction, this variational state obeys the single-occupancy constraints (1.18).

Since the overall phase of the state (2.2) is arbitrary, we will take λ to be real. We have introduced the ϕ_n so that we may also take the u and the v to be real.

The amplitude of the cavity mode is given by the expectation value $\langle \psi \rangle$, and the polarisation of the nth two-level oscillator by the expectation value $\langle b_n^\dagger a_n \rangle$. In the state (2.2) we have $\langle \psi \rangle = \lambda$ and $\langle b_n^\dagger a_n \rangle = u_n v_n e^{i\phi_n}$. Thus, in general, this state has both a finite amplitude of the cavity mode and a finite polarisation of the electronic states. The ϕ_n are the phase differences between the electronic polarisations and the electromagnetic field in the cavity.

As well as its application to superconductors, the BCS wavefunction contained in (2.2) has been widely used to describe Bose condensed excitons, particularly by Comte and Nozières [46]. As these authors stress, this wavefunction can describe Bose condensed excitons away from the low-density limit in which excitons are simple bosons (Eq. (1.5)): it allows for the fermionic structure of the exciton. In a similar way, it allows for the fermionic structure of the electronic excitations, i.e. the saturation nonlinearity, in the model (1.19).

2.2 MINIMISING THE FREE ENERGY

To find the ground state of (1.19) at fixed total excitation, we introduce a chemical potential μ_{ex} to constrain the excitation, and minimise

$$
\begin{aligned}
\langle H - \mu_{ex} L \rangle &= \tilde{\omega}_c \lambda^2 + \sum_n \tilde{\varepsilon}_n (v_n^2 - u_n^2) \\
&\quad + 2 \frac{g}{\sqrt{N}} \lambda u_n v_n \cos(\phi_n), \qquad (2.3) \\
\tilde{\omega}_c &= \omega_c - \mu_{ex}, \\
\tilde{\varepsilon}_n &= \frac{E_g(n) - \mu_{ex}}{2},
\end{aligned}
$$

with respect to the variational parameters, subject to the normalisation conditions $u_n^2 + v_n^2 = 1$.

Although the overall phase of the condensate is arbitrary, the relative phases ϕ_n are not: there is only one order parameter. The relative phases ϕ_n are fixed by the last term in (2.3), the dipole coupling. This term ensures that all the two-level oscillators which have a finite dipole moment$(u_n \neq 0, 1)$ are mutually coherent, $\phi_n = \phi$, when the energy is minimised.

Setting $\phi_n = 0$ and defining an intensive λ by rescaling $\lambda \to \lambda \sqrt{N}$, the minima of (2.3) are given by the real solutions with $\lambda u_n v_n < 0$ to

$$
\tilde{\omega}_c \lambda + \frac{g}{N} \sum_n u_n v_n = 0, \qquad (2.4)
$$

$$
2 \tilde{\varepsilon}_n u_n v_n - g \lambda (v_n^2 - u_n^2) = 0.
$$

We define an excitation density $\rho_{ex} = \langle L \rangle / N$, which is the total number of photons and electronic excitations, per two-level oscillator, minus one-half. Since the numbers of photons and electronic excitations are positive, the lowest excitation density is -0.5. Since the number of electronic excitations is always less than N, the electronic contribution to ρ_{ex} is always less than 0.5.

μ_{ex} is a Lagrange multiplier which constrains the excitation num-

ber. It is related implicitly to the excitation density by

$$\rho_{ex} = \frac{1}{N} \left\langle \psi^\dagger \psi + \frac{1}{2} \sum_n b_n^\dagger b_n - a_n^\dagger a_n \right\rangle$$
$$= \lambda^2 + \frac{1}{2N} \sum_n v_n^2 - u_n^2. \tag{2.5}$$

Eliminating u_n and v_n from (2.4) and (2.5) we can rewrite these expressions as

$$\tilde{\omega}_c \lambda = \frac{g^2 \lambda}{2N} \sum_n \frac{1}{|E_n|}, \tag{2.6}$$

$$\rho_{ex} = \lambda^2 - \frac{1}{2N} \sum_n \frac{\tilde{\varepsilon}_n}{|E_n|}, \tag{2.7}$$

where we define

$$E_n = \text{sign}(\tilde{\varepsilon}_n)\sqrt{\tilde{\varepsilon}_n^2 + g^2|\lambda|^2}. \tag{2.8}$$

(2.6) is analogous to the BCS gap equation, with an order parameter λ.

2.3 RESULTS

To investigate the expressions (2.6–2.8) we replace the summations over sites with an integral over an energy distribution for the two-level oscillators. We take this distribution to be a Gaussian with mean E_0 and variance σg. The remaining parameters in our quasi-equilibrium problem are then the excitation density, ρ_{ex}, and the dimensionless detuning between the photon frequency and the centre of the energy distribution of the two-level oscillators, $\Delta = (\omega_c - E_0)/g$.

For a Gaussian density of states, the summation on the right of (2.6) diverges as $\lambda \to 0$, and approaches zero as $\lambda \to \infty$. Thus for any $\mu_{ex} < \omega_c$ there is always a condensed solution, $\lambda \neq 0$, to (2.6): the system is condensed at arbitrarily small excitation densities. This behaviour is produced by the tails of the Gaussian distribution. Because of these tails, we have electronic excitations("excitons") at arbitrarily low energies, and hence also bound exciton-photon states at arbitrarily

34
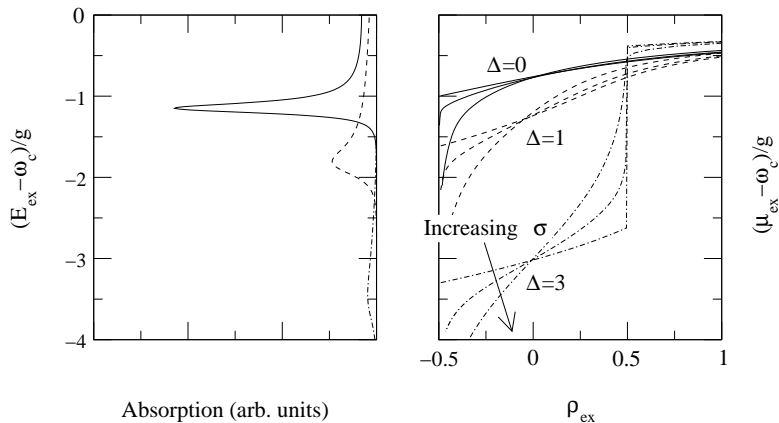
Figure 2.1: Right panel: dependence of the chemical potential on excitation density for detunings $\Delta = 0, 1$ and 3 and variances $\sigma = 0, 0.5$ and 1. Left panel: absorption spectrum for a microcavity at $\rho_{ex} = -0.5$ and $T = 0$ for $\sigma = 0.5$ and the same three detunings.

low energies. It is impossible to populate just the excitons, because, no matter how small μ_{ex} is, there is always a bound state involving photons below it. We expect that if the density of states has a lower cut-off, and is continous at this cut-off, there would be a finite critical μ_{ex} below which there is no condensed solution to (2.6).

Let us investigate the dependence of μ_{ex} on ρ_{ex} in the absence of inhomogeneous broadening, $\sigma = 0$. At low densities, $\rho_{ex} \approx -0.5$, μ_{ex} can be obtained from (2.6). Expanding this expression for small λ and comparing the leading terms, we find that μ_{ex} is given by the conventional bosonic polariton energy $\mu_{ex} = E_{\mathrm{LPB}} = \frac{1}{2}[(\omega_c + E_g) - g\sqrt{\Delta^2 + 4}]$. This confirms that, at low densities, we are describing a condensate of conventional bosonic polaritons. At finite densities we calculate μ_{ex} numerically, by solving (2.6) and (2.7) to determine $\rho_{ex}(\mu_{ex})$. The results are plotted in the right panel of Fig. 2.1, for $\Delta = 0, 1$ and 3. For a condensate of non-interacting bosonic polari-

35

tons we would have $\mu_{ex} = E_{\text{LPB}}$ at all densities. Here however, the electronic states saturate with increasing density, forcing the excitations to become more photon-like. Thus the chemical potential approaches ω_c at high densities. For $\Delta > 2$ the separation between the exciton-like and photon-like excitations persists to $\rho_{ex} = 0.5$, where the electronic excitations are completely saturated. This results in a discontinuity in μ_{ex} at this point, since no further excitation can be added to the electronic states.

The dependence of μ_{ex} on ρ_{ex} in the inhomogeneously broadened case is also illustrated in the right panel of Fig. 2.1. It is qualitatively rather similar to the homogeneous case. Instead of the finite intercept of the homogeneous case we now have $\mu_{ex} \to -\infty$ as $\rho_{ex} \to -0.5$; this behaviour is again caused by the tails of the Gaussian distribution. To demonstrate how μ_{ex} approaches the conventional polariton energy E_{LPB} in the homogeneous, low-density limit, we compare the behaviour of μ_{ex} with the density of states for the linear-response excitations of the empty($\rho_{ex} = -0.5$) cavity. This density of states is the optical absorption spectrum of the cavity, and is plotted in the left panel of Fig. 2.1 for $\sigma = 0.5$ and $\Delta = 0, 1$ and 3. We will describe how it is calculated in Chapter 4. At very low densities, μ_{ex} lies in the tails of the exciton distribution. With increasing density, these states quickly saturate, producing a sharp rise in μ_{ex}. As μ_{ex} reaches the polariton peak, the sharp rise in the density of states for the coupled modes produces a kink in the chemical potential. In the homogeneous limit, this kink moves to zero density and corresponds to the usual polariton energy. Since the density of states at this point is infinite in the homogeneous limit, these polaritons are bosons.

Figure 2.2 shows the occupation of the two-level oscillators in the polariton condensate, for $\Delta = 3, \sigma = 0.5$ and various densities. The occupation number of the nth two level oscillator is

$$\frac{1}{2}(v_n^2 - u_n^2 + 1) = \frac{1}{2}\left(1 - \frac{\tilde{\varepsilon}_n}{|E_n|}\right).$$

As is clear from the figure, this is a Fermi step broadened by the interaction with the photons, just as the electronic distribution in a BCS superconductor is a Fermi step broadened by the pairing interaction.
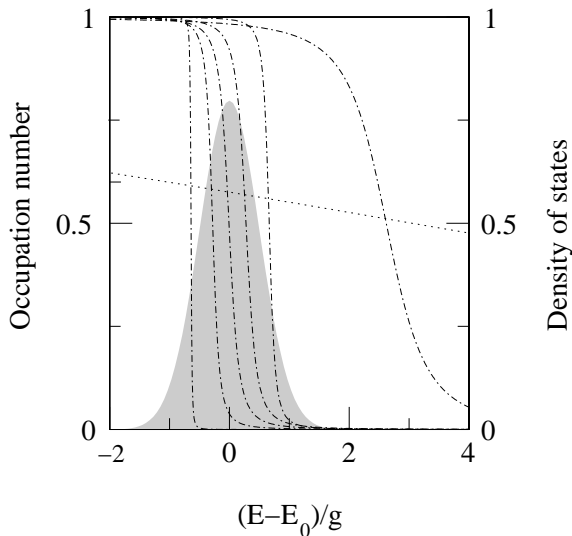
Figure 2.2: Occupation of the two-level oscillators at zero temperature as a function of energy E for $\Delta = 3$, $T = 0$, $\sigma = 0.5$ and densities $\rho_{ex} = -0.4, -0.2, 0, 0.2, 0.4, 0.6$(dot-dashed curves, increasing from left to right) and $\rho_{ex} = 100$(dotted curve). The shaded region shows the density-of-states for the bare electronic excitations.

The states in the broadened region of the step have a finite dipole moment and are involved in the condensate. The Fermi step moves up through the energy distribution of the two-level oscillators as the excitation is increased from $\rho_{ex} = -0.5$ and the low-lying electronic states saturate. At very large densities there are a large number of photons, and the Fermi step is almost completely flat. Rather than the electronic system completely saturating in the high density limit, it approaches half-filling. This is because the half-filled state maximises the polarisation of the electronic states and hence minimises the dipole interaction between the electronic states and the macroscopically occupied cavity mode.

Careful inspection of Fig. 2.2 reveals that the broadening of the Fermi step produced by the photons does not increase monotonically with density. This corresponds to a non-monotonic dependence of the
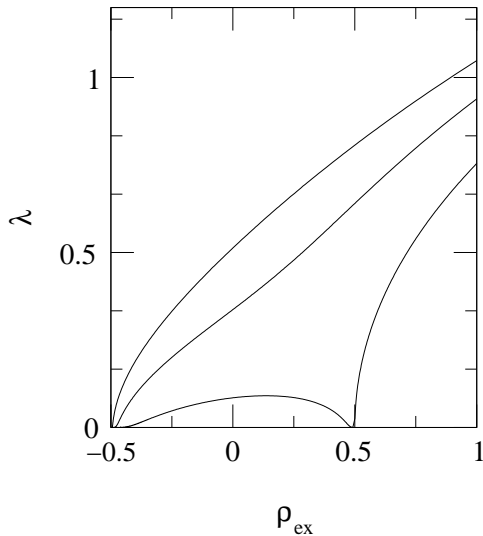
Figure 2.3: The order parameter λ as a function of density, for $\sigma = 0.5$ and $\Delta = 0$, 1 and 3. λ^2 is the photon number per two-level oscillator in the condensed state.

rescaled field amplitude λ on density. This dependence is illustrated in Fig. 2.3. The field amplitude is related to the electronic polarisation by the first of the equations (2.4). It is proportional to the electronic polarisation and inversely proportional to the separation between the chemical potential and the cavity mode. The electronic polarisation depends on the density of states in the vicinity of the chemical potential(Fig. 2.2); the peak in the density of states at the centre of the exciton line produces the peak in Fig. 2.3.

2.4 Conclusions

We have shown how the ground state of the Dicke model at low densities may be generalised to allow for the saturation nonlinearity and the inhomogeneous broadening. We found that, for the Gaussian density of states we have chosen, the ground state of the model at fixed L is always a condensate: neither the saturation nor the Gaussian broad-

38

ening prevent condensation. The condensed state we have found is characterised by coherence in both the photons and the electronic excitations. The latter is evident, for example, in the broadening of the Fermi distribution in figure 2.2. The presence of coherence in the electronic states is in marked contrast with a conventional laser, which has coherence in the photons but not in the gain medium. The rigid coherence which is characteristic of Bose condensates [41] is, in the present example, produced by the dipole coupling between the electronic excitations and the photons.

Chapter 3

AN EXACT SOLUTION AT FINITE TEMPERATURES

I$_N$ $_{THIS}$ $_{CHAPTER,}$ we investigate the thermal equilibrium of the model (1.19) at fixed excitation using a path-integral technique. In this technique, the partition function is written as a functional integral, which can be evaluated for large N using a standard saddle-point approach[1]. This gives a more rigorous derivation of the variational equations (2.6–2.8), and demonstrates that the variational description is essentially exact in the limit $N \to \infty$. Furthermore, it generalises the variational equations to finite temperatures, and allows us to investigate the phase diagram of our quasi-equilibrium problem.

The path-integral techniques used in this Chapter have previously been used [49, 51] to calculate the partition function and excitation energies *in the absence of a constraint on the excitation number* of a simplification of the Dicke model (1.15). While the Hamiltonian of the simplified model discussed in Refs. [49, 51] is given by (1.19) with $E_g(n) = E_g$, the local constraint prohibiting two fermions on the same site, (1.18), is replaced with a global constraint. In contrast, we retain (1.18) as local constraints, as well as including a distribution of E_g and a constraint on the excitation number.

Physically, the reason why the variational approach of Chapter 2 becomes exact as $N \to \infty$ is that it corresponds to a mean-field treatment of the interaction between electronic excitations. This interaction, between a large number (N) of electronic excitations, is mediated by a small number (one) of cavity modes. In the mean-field

---

[1] For general discussions of path-integrals, and saddle-point techniques for their evaluation, see e.g. Refs. [47–50]; for an introduction to their application to interacting systems of light and matter, see Ref. [49].

treatment, each electronic excitation is coupled to the average field produced in the cavity by the other electronic excitations. Replacing the field in the cavity with its average value is justified because, when there are a large number of electronic excitations contributing to a small number of field modes, the fluctuations of the field will be negligible.

The basic idea behind the mathematics of this chapter is to construct the free energy in powers of N. The mean-field equations (2.6-2.8), generalised to finite temperatures, are obtained by considering the terms in the free energy which are proportional to N.

3.1   Path-integral Formulation

As in the previous chapter, we work in a grand-canonical ensemble, using a chemical potential μ_{ex} to constraint the excitation L. We consider the partition function associated with this ensemble,

$$Q = \operatorname{Tr} e^{-\beta(H - \mu_{ex}L)}.$$

The coherent-state path-integral formalism expresses this partition function, for the model (1.19), as the constrained functional integral

$$Q = \int \mathcal{D}\psi \prod_n [\mathcal{D}\eta_n \delta(\bar{\eta}_n \eta_n - 1)] e^{-S},$$

with the action

$$S = \int_0^\beta d\tau \, \bar{\psi}(\partial_\tau + \tilde{\omega}_c)\psi + \sum_n \bar{\eta}_n M_n \eta_n.$$

We have introduced Nambu spinors

$$\eta_n = \begin{pmatrix} b_n \\ a_n \end{pmatrix}$$

42

on each fermion site to simplify the notation. The matrix M_n is

$$M_n = \begin{pmatrix} \partial_\tau + \tilde{\varepsilon}_n & g\psi/\sqrt{N} \\ g\bar{\psi}/\sqrt{N} & \partial_\tau - \tilde{\varepsilon}_n \end{pmatrix}.$$

Rescaling the boson field $\psi \rightarrow \sqrt{N}\psi$ and transferring the fermionic integrals into the action gives

$$Q = \int \mathcal{D}\psi |J| e^{-NS_{\text{eff}}},$$

with an effective action

$$
\begin{aligned}
S_{\text{eff}} &= \int_0^\beta d\tau \bar{\psi}(\partial_\tau + \tilde{\omega}_c)\psi - \frac{1}{N}\sum_n S_{\text{f},n}, & (3.1) \\
S_{\text{f},n} &= \ln \int \mathcal{D}\eta_n \delta(\bar{\eta}_n \eta_n - 1) e^{-\int_0^\beta \bar{\eta}_n P_n \eta_n},
\end{aligned}
$$

in which the P_n are the matrix operators M_n after rescaling the boson field, and J is the trivial Jacobian produced by this rescaling.

3.2 THE EXTREMAL EQUATION

For large N, the dominant contribution to the partition function Q comes from the functions $\psi_0(\tau)$ which minimise the functional S_{eff}. Provided that they are sufficiently smooth [52], such functions obey the Euler-Lagrange equation. For the action (3.1), this takes the form

$$
\begin{aligned}
(\partial_\tau + \tilde{\omega}_c)\psi_0(\tau) &= \frac{1}{N}\sum_n \frac{\delta S_{\text{f},n}}{\delta\bar{\psi}}\bigg|_{\psi(\tau)=\psi_0(\tau)} \\
&= -\frac{g}{N}\sum_n \langle \bar{a}_n(\tau)b_n(\tau)\rangle, & (3.2)
\end{aligned}
$$

where the right-hand side of this expression is the polarisation of a set of two-level oscillators in thermal equilibrium driven by an external field $\psi_0(\tau)$. This polarisation can be finite because the field $\psi_0(\tau)$ modifies the eigenstates [53] of the electronic system. A thermal population of these new eigenstates can correspond to a finite polarisation

43

of the original fermions. Equation (3.2) is a self-consistency condition: the electromagnetic field is driven by the polarisation of the fermions, which itself arises from the renormalisation of the fermions produced by the photons.

Assuming a stationary solution, $\psi_0(\tau) = \lambda$, we calculate the polarisation term on the right of (3.2) by making a Bogolubov transformation

$$\eta_n = \left(\begin{array}{cc} \cos(\theta)e^{i\phi} & -\sin(\theta) \\ \sin(\theta) & \cos(\theta)e^{-i\phi} \end{array} \right) \left(\begin{array}{c} \delta_n \\ \gamma_n \end{array} \right) \tag{3.3}$$

from the a_n and b_n fermions to new fermions γ_n and δ_n. This transformation diagonalises P_n when $\phi = \arg \lambda$ and $\tan 2\theta = g|\lambda|/\tilde{\varepsilon}_n$. The δ_n and γ_n quasiparticles then have energies $\pm E_n$ respectively, with E_n defined by equation (2.8). Since (3.3) is a rotation in η space, it preserves the single occupancy constraints. Thermally populating the γ_n and δ_n in accordance with the single occupancy constraint we have

$$\begin{aligned} \langle \bar{a}_n b_n \rangle &= \frac{1}{2} e^{i\phi} \sin(2\theta) \langle \bar{\delta}_n \delta_n - \bar{\gamma}_n \gamma_n \rangle \\ &= \frac{1}{2} e^{i\phi} \sin(2\theta) \tanh(\beta E_n), \end{aligned}$$

and (3.2) becomes

$$\tilde{\omega}_c \lambda = \frac{g^2 \lambda}{2N} \sum_n \frac{1}{E_n} \tanh\left(\beta E_n\right). \tag{3.4}$$

Equation (3.4) is the finite-temperature generalisation of the variational result (2.6). This generalisation is rather straightforward: we have just acquired a $\tanh(\beta E)$ factor to describe the thermal excitation of the two-level oscillators.

If we remove the constraint on the polariton number, by setting $\mu_{ex} = 0$, and set $E_g(n) = E_g$, then (3.4) is the form originally derived by Hepp and Lieb [44], and since rederived by many others, for the unconstrained equilibrium of the Dicke model (1.15).

In the unconstrained problem considered by Hepp and Lieb, the

44

existence of a condensed solution, $\lambda \neq 0$, requires

$$\frac{\omega_c E_g}{g^2} < 1, \tag{3.5}$$

which follows from (3.4) with $\mu_{ex} = 0$ and $E_g(n) = E_g$. However, it is shown in Refs. [54] and [55] that the A^2 terms of the minimal coupling Hamiltonian, neglected in the model (1.15), modify the inequality (3.5) in a way which is inconsistent with the Thomas-Kuhn-Reich sum rule. This sum rule requires $\kappa E_g/g^2 > 1$, where κ is the coupling constant for the A^2 term, while the modified inequality (3.5) reads

$$\frac{(\omega_c + 2\kappa)E_g}{g^2} < 1. \tag{3.6}$$

Since this inequality cannot be satisfied, the phase transition in the unconstrained case is an unphysical artifact of the model (1.15). However, we do not believe that the A^2 terms will prevent condensation in the constrained problem, because the inequality corresponding to (3.6) will be

$$\frac{(\tilde{\omega}_c + 2\kappa)(E_g - \mu_{ex})}{g^2} < 1,$$

and the parameter μ_{ex} is not restricted by the sum rule.

3.3 EFFECT OF FLUCTUATIONS

Let us now consider the effect of small fluctuations $\delta\psi(\tau)$ around the mean-field solution. Expanding S_{eff} to second order in a functional Taylor series around the mean-field solution we have

$$Q \approx e^{-NS_0} \int \mathcal{D}(\delta\psi)|J|e^{-NS_2[\delta\psi,\bar{\delta\psi}]}. \tag{3.7}$$

Here S_0 is the action evaluated on the extremal trajectory and S_2 is the quadratic action from the second order term in the Taylor series. S_2 is the effective action for small fluctuations of the electromagnetic field. The kernel of S_2, $\mathcal{G}^{-1}$, is the inverse of the thermal Green's function for the photons.

The integral over fluctuations in (3.7) contributes a term

$$\frac{1}{N} \ln \det \mathcal{G}^{-1}$$

to the free energy density. Since the mean-field solution should be a minimum of the action, the eigenvalues of $\mathcal{G}^{-1}$ should be positive. Then $\ln \det \mathcal{G}^{-1}$ is finite as $N \to \infty$, there is no fluctuation contribution to the free energy density in this limit, and the mean-field theory becomes exact.

3.4 Effective Action for Fluctuations

However, we have yet to check whether the solutions to (3.4) are actually minima of the action or merely extrema, i.e. whether the mean-field solutions are stable against fluctuations. To check this, we will need the effective action S_2, which we derive in this section.

To obtain S_2, we calculate the (functional) second derivatives of S_{eff}, and evaluate them on the extrema $\psi(\tau) = \psi_0(\tau) = \lambda$. This relates S_2 to the two-time correlation functions for a set of two-level oscillators in an external field λ. We work in frequency space, using ω and ω' to denote bosonic Matsubara frequencies. Because we are working with a condensed system we find both normal,

$$\frac{\partial^2 S_{\text{eff}}}{\partial \psi(\omega) \partial \bar{\psi}(\omega')} = \beta \delta(\omega' - \omega) \bigg[i\omega + \tilde{\omega}_c \tag{3.8}$$

$$-\frac{g^2}{N} \sum_n \int_0^\beta e^{-i\omega\tau} (\langle \sigma_n^-(\tau) \sigma_n^+(0) \rangle$$

$$- \langle \sigma_n^- \rangle \langle \sigma_n^+ \rangle) \bigg] d\tau,$$

and anomalous,

$$\frac{\partial^2 S_{\text{eff}}}{\partial\psi(\omega)\partial\psi(\omega')} = \quad -\beta g^2 \delta(\omega' + \omega) \tag{3.9}$$

$$\times \frac{1}{N} \sum_n \int_0^\beta e^{i\omega\tau} (\langle \sigma_n^+(\tau)\sigma_n^+(0)\rangle$$

$$- \langle \sigma_n^+ \rangle \langle \sigma_n^+ \rangle) d\tau,$$

contributions to S_2. The latter describe fluctuations which do not conserve the number of excitations out of the condensate; i.e. those in which an excitation either enters or leaves the condensate. Here $\sigma_n^+ = b_n^\dagger a_n$ excites the nth two-level oscillator.

The integrands in (3.8) and (3.9) are the self-consistent susceptibilities of the electronic system; these equations describe coupled fluctuations of the cavity field and the electronic polarisation. They are analogous to the Dyson-Gor'kov-Beliaev equations [49] of superconductivity and the theory of weakly-interacting Bose gases.

Calculating the electronic susceptibilities which appear in (3.8) and (3.9) by directly solving the imaginary-time Heisenberg equation

using the transformation (3.3), we find for S_2

$$S_2[\delta\psi, \delta\bar{\psi}] = \beta \sum_{\omega} \left(\begin{array}{cc} \delta\bar{\psi}(\omega) & \delta\psi(-\omega) \end{array} \right) \mathcal{G}^{-1} \left(\begin{array}{c} \delta\psi(\omega) \\ \delta\bar{\psi}(-\omega) \end{array} \right),$$

$$\mathcal{G}^{-1} = \left(\begin{array}{cc} K_1 & K_2 \\ K_2^* & K_1^* \end{array} \right), \qquad (3.10)$$

$$K_1 = i\omega + \tilde{\omega}_c + \frac{g^2}{N} \sum_n \left[\frac{1}{E_n} \tanh(\beta E_n) \right.$$

$$\left. \times \frac{i\tilde{\varepsilon}_n\omega - 2\tilde{\varepsilon}_n^2 - g^2|\lambda|^2}{\omega^2 + 4E_n^2} + \delta_\omega \alpha_n |\lambda|^2 g^2 \right],$$

$$K_2 = \frac{g^4\lambda^2}{N} \sum_n \left[\frac{1}{E_n(\omega^2 + 4E_n^2)} \tanh(\beta E_n) \right.$$

$$\left. + \delta_\omega \alpha_n \right],$$

$$\alpha_n = -\frac{\beta}{4E_n^2} \text{sech}^2(\beta E_n).$$

Note that, for the condensed state, $\mathcal{G}^{-1}$ takes different forms at $\omega = 0$ and at finite ω. This is because thermal fluctuations at $\omega = 0$ include both fluctuations of the order parameter and quasiparticle excitations [56]. Only the latter appear at finite ω. In the normal state, $\lambda = 0$, the effective action simplifies to

$$S_2 = \beta \sum_\omega \delta\bar{\psi}(\omega) \left[i\omega + \tilde{\omega}_c \right.$$

$$\left. + \frac{1}{N} \sum_n \frac{g^2 i}{\omega - 2i\tilde{\varepsilon}_n} \tanh(\beta \tilde{\varepsilon}_n) \right] \delta\psi(\omega). \qquad (3.11)$$

3.5 Nature of the Extrema

We now use the expressions (3.10–3.11) to investigate the nature of the extrema for the homogeneous model $E_g(n) = E_g$.

Considering first a condensed solution, $\lambda \neq 0$, we use the extremal equation (3.4) to eliminate $\frac{1}{E_n} \tanh(\beta E_n)$ from the matrix $\mathcal{G}^{-1}$. The

eigenvalues of the resulting matrix are all strictly positive provided that $\tilde{\omega}_c > 0$, except for a single zero eigenvalue at $\omega_n = 0$. From (3.4) we see that the condensed solutions always have $\tilde{\omega}_c > 0$. Thus we conclude that, at a condensed solution, the action has a minimum in all but one direction, and is locally flat in this one direction.

We show in Appendix A that the single zero eigenvalue describes a change in the overall phase of the condensate. It is the Goldstone mode corresponding to the broken gauge symmetry of the condensate. Because we are considering a broken symmetry state, we should not integrate over these fluctuations when calculating the partition function. Since the other eigenvalues of $\mathcal{G}^{-1}$ are always positive for the condensed solutions, these solutions are stable against physical fluctuations, and the mean-field theory is exact[2].

Turning now to the normal solution, $\lambda = 0$, we find from (3.11) that this is a minimum of the action unless

$$\tilde{\omega}_c < \frac{g^2}{2\tilde{\varepsilon}} \tanh(\beta\tilde{\varepsilon}). \qquad (3.12)$$

This is just the condition for the extremal equation (3.4) to have a condensed solution. Thus we have the usual scenario of a continuous phase transition: there is a phase boundary (3.12), at which the normal state becomes unstable and a stable, condensed solution appears.

3.6   THE DENSITY EQUATION

In addition to the mean-field equation (3.4), we need the equation relating the density ρ_{ex} to the corresponding chemical potential μ_{ex}. This is related to the partition function in the standard way,

$$\rho_{ex} = \frac{1}{\beta N} \frac{\partial}{\partial \mu_{ex}} \ln Q. \qquad (3.13)$$

The asymptotic form for the partition function is $Q \sim e^{-NS_0}$, where S_0 is the minimal action. Inserting this asymptotic form in (3.13)

---

[2]In Appendix A, we give a formal demonstration that the zero mode does not contribute to the free energy density as $N \to \infty$, so that the discussion of section 3.3 continues to apply.

gives, for the stationary solution $\psi_0(\tau) = \lambda$,

$$\rho_{ex} = |\lambda|^2 - \frac{1}{2N} \sum_n \frac{\tilde{\varepsilon}_n}{E_n} \tanh\left(\beta E_n\right), \qquad (3.14)$$

which is the generalisation of (2.7) to finite temperatures.

The first term in (3.14) is the contribution to the excitation density from the macroscopic electromagnetic field, while the second term is the contribution from the thermal population of renormalised electronic excitations. In the absence of a macroscopic electromagnetic field, $\lambda = 0$, both the photon contribution to ρ_{ex} and the renormalisation effects vanish. The expression (3.14) is then the familiar form for the excitation of a set of two-state oscillators.

3.7 The Result: A Phase Diagram

From (3.12) and (3.14) we have the critical temperature for condensation, as a function of the excitation density, in the homogeneous model. This critical temperature is

$$\beta_c g = \frac{4 \tanh^{-1}(2\rho_{\text{ex}})}{\Delta \pm \sqrt{\Delta^2 - 8\rho_{ex}}}. \qquad (3.15)$$

Note that the transition temperature depends logarithmically on the density, and its scale is set by the interaction strength g. This is in contrast to a model of propagating, weakly-interacting bosons. In that model, the transition temperature varies as a power law of the density and its scale is set by the mass of the bosons.

At low densities, (3.15) is the phase boundary separating a population of electronic excitations with energy E_0 from a population of conventional bosonic polaritons with energy

$$E_{\text{LPB}} = \frac{1}{2}\left[(\omega_c + E_0) - g\sqrt{\Delta^2 + 4}\right].$$

To see this, note that this transition would occur when the chemical potential for the electronic excitations reaches E_{LPB}, corresponding to a density $\rho_{ex} + 0.5 \approx e^{-\beta_c(E_0 - E_{LPB})}$, which is the low-density limit
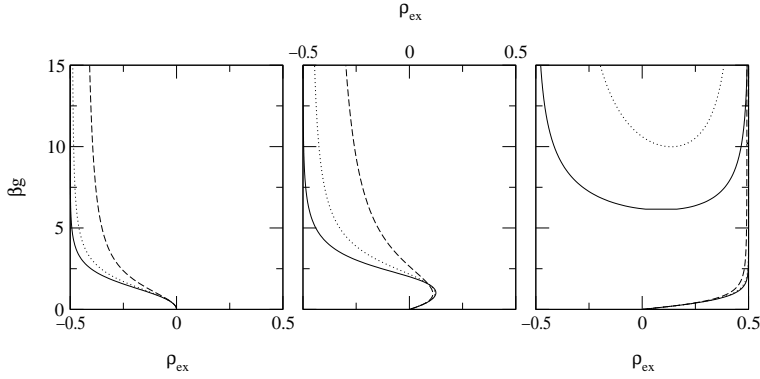
Figure 3.1: Phase boundaries for $\Delta = 0$(left panel), $\Delta = 1$(centre panel) and $\Delta = 3$(right panel), and variances $\sigma = 0$(solid lines), $\sigma = 0.5$(dotted lines) and $\sigma = 1$(dashed lines). For $\Delta = 3$, $\sigma = 1$ the upper branch of the phase boundary lies off the scale, while for $\Delta = 3$, $\sigma = 0.5$ the lower branch is indistinguishable from the homogeneous case.

of (3.15).

From the discussion of equation (3.12), we know that the homogeneous model has a continuous transition between the normal and condensed states. We can obtain the phase boundary for the inhomogeneous model by assuming that it too has a continuous phase transition. With this assumption, the phase boundary $\mu_c(\beta_c)$ is given by demanding that (3.4) have a repeated root $\lambda = 0$. Equation (3.14) then gives $\rho_c(\beta_c)$. We follow this procedure numerically, assuming the same Gaussian distribution for the exciton states as in section 2.3.

In Fig. 3.1 we plot the homogeneous phase boundaries (3.15), along with our numerical results for the inhomogeneous model with $\sigma = 0.5$ and 1. On resonance, $\Delta = 0$, the transition temperature monotonically increases with density. The system is always condensed for $\rho_{ex} > 0$, because to exceed this density would require a chemical potential above the centre of the energy distribution of the electronic excitations, and hence above the bosonic cavity mode. While for $\Delta < 0$(not illustrated) the phase boundary is qualitatively unchanged from the resonant case, for $\Delta > 0$ we find reentrant behaviour. This

51
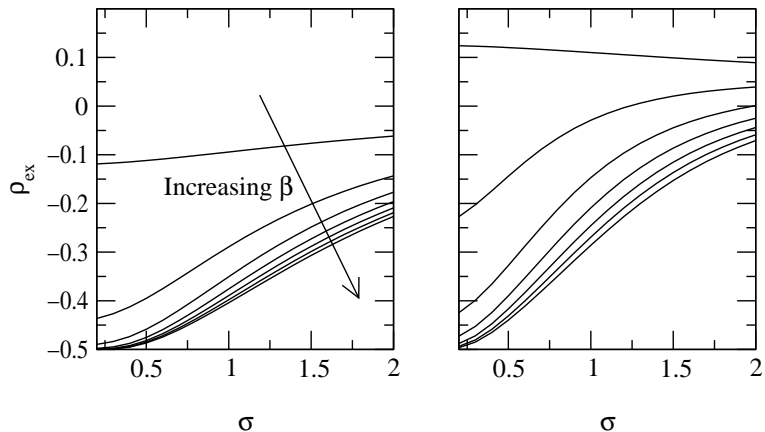
Figure 3.2: Dependence of the critical density on the inhomogeneous broadening σ, for $\Delta = 0$(left panel) and $\Delta = 1$(right panel), and $\beta = 1$(top curve), 3, 5, 7, 9, 11, 13(lowest curve).

behaviour is the result of the saturable nature of the electronic states. It can be understood by considering the limits $\rho_{ex} \rightarrow \pm 0.5$ when $\Delta \gg 0$. Near the $\rho_{ex} = -0.5$ limit, the normal state consists of a small number of electronic excitations weakly interacting through the cavity mode. They condense when their density exceeds a critical value set by the strength of the effective interaction, determined by Δ and g. Near the $\rho_{ex} = 0.5$ limit, the electronic system is constrained to be fully occupied, and the normal state consists of a small number of holes in an otherwise completely excited electronic system. These holes again interact through the photon field, and so the transition occurs when the density of holes, $0.5 - \rho_{ex}$, exceeds a critical value. For $\Delta \rightarrow \infty$ the critical densities of holes and excitons are identical, so the phase diagram is symmetric about $\rho = 0$. For finite Δ the effective interaction is stronger for the holes than for excitons, since they are nearer in energy to the cavity mode, and so the phase boundary becomes skewed to the forms illustrated.

At temperatures which are high compared with the inhomogeneous broadening σg, thermal fluctuations dominate over the inhomogeneous linewidth. Thus at these temperatures the inhomogeneous broaden-

ing has little effect, as can be seen in Fig. 3.1. However, at low temperatures the inhomogeneous broadening suppresses condensation by increasing the energy separation between the material excitations and the photon mode, and so collapsing the phase boundaries towards $\rho_{ex} = 0$. The effects of inhomogeneous broadening are further illustrated in Fig. 3.2, which shows the dependence of the critical density on σ at various temperatures for detunings $\Delta = 0$ and $\Delta = 1$.

3.8 Conclusions

By rederiving the variational equations (2.6–2.8) from an expansion of the partition function in $1/N$, we have generalised these equations to finite temperatures, and shown that they become exact as $N \to \infty$. We have seen that the polariton condensate is formed from a thermalised population of electronic excitations, whose energies are renormalised by the self-consistent field in the cavity. We have constructed the phase diagram of the model (1.19) at fixed excitation, and found a phase boundary which is very different from that of the weakly-interacting Bose gas; in particular, the scale of our critical temperature is set by the interaction strength g. The phase boundary displays unusual features (reentrance) due to the saturable nature of the electronic states.

Chapter 4

THE EXCITATION SPECTRA

IN THIS CHAPTER, we use the expressions derived in section 3.4 to study the excitation spectrum of the quasi-equilibrium states of the model (1.19). The excitation spectra we calculate explain the form of the phase diagrams in figure 3.1. The excitation spectra of the two quasi-equilibrium states are different from each other, and also from the excitation spectrum of a conventional laser. Since the excitation spectrum is directly related to the optical absorption spectrum of the cavity, which is an experimentally accessible quantity, these spectra offer a clear experimental signature of polariton condensation.

The matrix $\mathcal{G}^{-1}$, given by (3.10), is the inverse of the thermal Green's function for the photons. We use the standard relations [50, 56] between thermal Green's functions, retarded Green's functions, and excitation spectra, to extract the excitation spectra from (3.10).

4.1 HOMOGENEOUS MODEL

We begin with the normal state of the homogeneous model. The inverse of the normal state Green's function contained in (3.11) can be written as a sum of simple poles

$$\mathcal{G}(\omega_n) = \frac{C_+}{i\omega_n + E_+} + \frac{C_-}{i\omega_n + E_-}. \tag{4.1}$$

The structure of this Green's function is clear: we have two excitations, with quasiparticle energies

$$E_\pm + \mu_{\mathrm{ex}} = [(\omega_c + E_g) \pm g\sqrt{\Delta^2 - 8\rho_{\mathrm{ex}}}]/2,$$

and corresponding weights

$$C_\pm = \pm(2\tilde{\varepsilon} - E_\pm)/(E_- - E_+).$$

These normal-state excitations are polaritons in the sense of Hopfield [1]: coupled modes involving the linear response of the electronic system around its equilibrium state. The gap in the spectrum is increased over the bare detuning Δ owing to the dipole coupling between the excitons and the cavity mode. The presence of excitation in the ground state, either driven by finite temperatures or by finite μ_{ex}, causes the two polariton branches to attract. This attraction is due to the decrease in the polarisability of the electronic states as their population increases and saturation occurs. It can also be understood in terms of an angular momentum representation [26] for the collective states of the electronic system. The excitation of the electronic states S_z forms the z component of an angular momentum and their polarisation forms a raising operator S_+. Thus the polarisability of the electronic states is maximised at $\langle S_z \rangle = -N/2$.

Since condensation is a phase transition, we expect a qualitatively different excitation spectrum in the condensed state. From (3.10) and (3.4), we find for the leading component of the matrix thermal Green's function

$$\mathcal{G}_{11}(i\omega_n) = \frac{\tilde{\omega}_c(\omega^2 + 2g^2|\lambda|^2) - i\omega(\omega^2 + 4E^2 + 2\tilde{\omega}_c\tilde{\varepsilon})}{(i\omega_n)^2(i\omega_n + \xi)(i\omega_n - \xi)(1 + \delta_{\omega_n}\alpha)}, \qquad (4.2)$$

with $\xi = \sqrt{(\tilde{\omega}_c + 2\tilde{\varepsilon})^2 + 4g^2|\lambda|^2}$.

The interpretation of this Green's function is complicated because, as we have already mentioned, it describes both quasiparticle excitations and fluctuations of the order parameter. To rigorously obtain the quasiparticle spectrum, we should extract the contribution to (4.2) from the order parameter fluctuations, and analytically continue the remainder to obtain the retarded Green's function. Rather than follow this procedure, we propose the following physically appealing if mathematically naïve interpretation of (4.2): the Kronecker delta and the $(i\omega_n)^2$ terms in the denominator describe the condensate response, leaving quasiparticle excitations at energies $\pm\xi$. The $(i\omega_n)^2$ is clearly

associated with the phase mode of the condensate, discussed in Appendix A, while the Kronecker delta is related to number fluctuations of the condensate [57]. The excitations at energy $\pm\xi$ are coupled exciton-photon modes in the presence of the macroscopic electromagnetic field of the condensate. ξ is analogous to the pair breaking energy in a superconductor: it is the energy required to extract an exciton-photon complex from the condensate. Note that if we remove the photon contribution to this energy, by setting $\tilde{\omega}_c = 0$, ξ becomes the familiar expression [53] for the energy of an electron-hole pair in the presence of an external macroscopic electromagnetic field at frequency μ_{ex}.
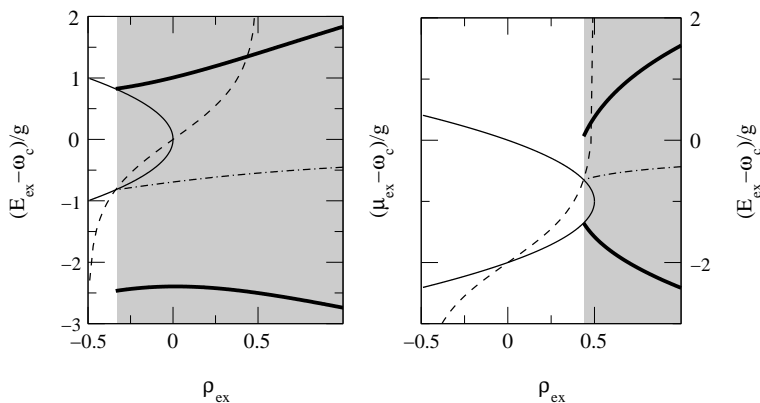
Figure 4.1: Excitation energies and normal state chemical potential as a function of density for the homogeneous model at $\Delta = 0$ (left panel) and $\Delta = 2$ (right panel), both with $g\beta = 2$. Thin solid lines: normal state excitation energies. Thick solid lines: condensed state excitation energies. Dashed lines: normal state chemical potential. Dot-dashed line: condensed state chemical potential. The shading marks the condensed region for this β.

In Fig. 4.1, we illustrate the evolution of the excitation energies of the microcavity with increasing density. To explain the relationship between the excitation energies and the phase diagram, we also plot the chemical potentials for the normal and condensed states on this figure. The left panel of this figure should be compared to the $g\beta = 2$

line of the corresponding phase diagram in Fig. 3.1.

When $\Delta = 0$ and $\rho_{\mathrm{ex}} = -0.5$ the system is in the normal state. Increasing ρ_{ex} populates the electronic excitations, increasing the chemical potential and decreasing the polariton splitting. Eventually the chemical potential crosses the lower polariton branch from below and the system condenses. At the critical density, the lower polariton branch joins to the phase mode at the chemical potential, while the upper branch joins to the "pair breaking" excitation. The excitation which appears below the chemical potential has zero weight at the transition. It corresponds to an excited state to ground state transition, where an exciton-photon complex is absorbed into the condensate. There is no corresponding excitation in the normal state Green's function, because the ground state of the $N+1$ particle system($N+1$ excitons) cannot be reached from the excited states of the N particle system($N-1$ excitons and 1 polariton) by adding a photon.

The relationship between the excitation spectrum and the phase diagram is slightly different when the transition occurs for $\rho_{ex} > 0$. For example, in the right panel of Fig. 4.1 the chemical potential crosses the lower polariton branch at $\rho_{\mathrm{ex}} = 0$ without the condensate appearing. It is not until the chemical potential crosses the upper polariton branch that the transition occurs. This can be understood by considering the signs of the quasiparticle weights $C_{\pm}$. A positive quasiparticle weight corresponds to absorption of an external field(a particle-like transition), whereas a negative quasiparticle weight corresponds to gain(a hole-like transition). For $\rho_{\mathrm{ex}} > 0$, the lower polariton branch has a negative weight: it has become hole-like, and must be below the chemical potential for stability. At the transition it is now this lower branch which joins to the "pair forming" excitation of the condensate, while the upper branch joins to the phase mode and the "pair breaking" excitation appears above the phase mode.

4.2 Inhomogeneous Model

In the inhomogeneous model, the discrete excitation spectrum of the homogeneous model is replaced by a continuous distribution of excitation energies. Thus we study the spectral density of excitations, $A(\omega)$.

The spectral density is related to the imaginary part of the retarded Green's function by

$$A(\omega) = 2\Im G^R(-\omega + \mu_{ex}). \qquad (4.3)$$

It is proportional to the linear absorption coefficient of the cavity at frequency ω, i.e. the imaginary part of the dielectric susceptibility.

To obtain $A(\omega)$ we require the retarded Green's function G^R. In the normal state this is given by the straightforward analytical continuation

$$G^R(\omega) = \lim_{\eta \to 0^+} \mathcal{G}(i\omega_n = \omega - i\eta). \qquad (4.4)$$

However, in the condensed state we face the mathematical difficulties already discussed for the homogeneous case. We avoid these difficulties by simply assuming that the continuation (4.4) of the normal state Green's function also applies in the condensed state.

Inverting the $\mathcal{G}^{-1}$ contained in (3.10) and using (4.3) and (4.4) expresses $A(\omega)$ in terms of integrals over the exciton distribution. We evaluate these integrals in the limit $\eta \to 0$ by setting $\eta = 0$ in the integrands and deforming the contour of integration around the poles of the integrand on the real axis. The contribution to the integrals from the detour around the poles can be performed analytically, leaving a principal value integral which we evaluate numerically[1]. We again assume a Gaussian distribution for the exciton energies.

Figure 4.2 shows the evolution of our calculated absorption spectra, $A(\omega)$, as we increase the density through the transition, for $g\beta = 2$, $\sigma = 1$, and $\Delta = 0$. The corresponding chemical potential is marked as the dashed line. Near to zero density our calculations reproduce the broadened polariton spectrum of Houdré et al.[29]. Comparison with Fig. 4.1 emphasises that the positions of the polariton peaks are largely unchanged from the homogeneous case. However, since the polariton energies are now resonant with a significant density of

---

[1]This is the same procedure that leads to the standard identity

$$\lim_{\eta \to 0^+} \frac{1}{x \pm i\eta} = \mathcal{P}\frac{1}{x} \mp i\pi\delta(x).$$
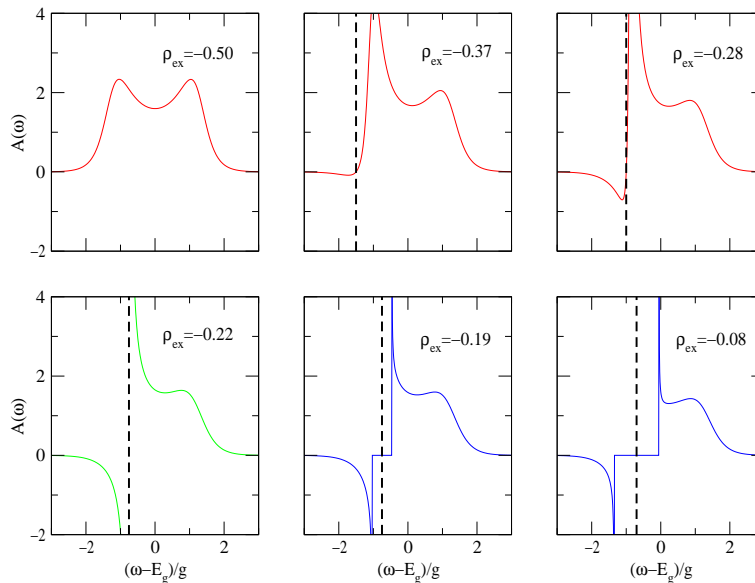
Figure 4.2: Spectral functions $A(\omega)$ for $\Delta = 0$, $g\beta = 2$, $\sigma = 1$ and chemical potentials $(\mu_{ex} - E_g)/g = -5, -1.5, -1.0, -0.76, -0.75, -0.70$, increasing from top left to bottom right through the transition at $(\mu_{ex} - E_g/g = -0.76)$. The top row of plots(red curves) are in the normal state, the bottom left hand plot(green curve) at the transition and the remaining plots(blue curves) in the condensed state. The dashed lines mark the chemical potential.

electronic states they become broadened. Increasing the chemical potential, but remaining in the normal state, we observe the thermal occupation factors producing gain below the chemical potential and increased absorption just above. The collapse of the polariton splitting evident in Fig. 4.1 is hardly noticeable at these low densities. As the density is increased still further a pole appears in $A(\omega)$ at the chemical potential; this marks the onset of condensation. Above the critical density the coherent photon field, oscillating at frequency μ_{ex}, produces a gap of magnitude $4g|\lambda|$ in the spectrum. The peak on the high energy side of the gap connects smoothly to the upper polariton

peak of the normal state, just as in the homogeneous case. In the homogeneous case we noted the appearance of an excitation below the chemical potential as we crossed the transition. This is still present in the inhomogeneous case, but in Fig. 4.2 it is far too weak to be visible.

4.3 CONCLUSIONS

We have calculated the excitation energies, and hence the absorption spectra, of the quasi-equilibrium states of the model (1.19). In the normal state the absorption spectrum resembles the conventional two-peaked polariton spectrum, although the splitting may be reduced due to the saturation nonlinearity and gain can appear below the chemical potential due to the thermal occupations of the electronic states.

The absorption spectrum in the condensate displays a gap, of magnitude $\sim g|\lambda|$, around the chemical potential. This gap is a manifestation of the renormalisation of the electronic states produced by the coherent photons. In a conventional laser this renormalisation is negligible, and there is no gap in the spectrum. Thus the presence or absence of a gap in the absorption spectrum is a clear, experimentally accessible, distinction between condensation and lasing.

It is interesting to note that the non-equilibrium analog [58] of the crossover illustrated in Fig. 4.1 and Fig. 4.2, from a two-peaked polariton spectrum to a "Stark triplet", has been observed experimentally in Ref. [59]. In this experiment, the gapped absorption spectrum is observed simultaneously with a short-pulse excitation. Thus there is no thermalisation involved in producing this spectrum. It is the result of coherence in the excitation pulse, rather than the spontaneous coherence of condensation. Nonetheless, these experiments demonstrate that the renormalisation of the electronic states which is essential to the present work can be realised experimentally.

61

Chapter 5

Concluding Remarks

Real microcavities are far more complex than the idealised model (1.19). However, like our model, they consist of photons coupled to electronic excitations which are bosons at low densities, but reveal their fermionic internal structure at high densities. Our work shows how the polariton condensate can be generalised to allow for such fermionic internal structures. Away from the low-density limit our generalised polaritons are not simple bosons. Their fermionic internal structure, i.e. the saturation nonlinearity, produces phenomena including (1)a collapse of the splitting between the peaks in the absorption spectrum of the normal state with increasing density, (2)a shift of the chemical potential of the condensate away from the conventional bosonic polariton energy, and (3)an unusual reentrant phase boundary for condensation. But it does not preclude condensation.

The experimental work reported in Refs. [34–38, 60], on the quantum statistical behaviour of polaritons, has focussed on low densities. This is to avoid effects due to the fermionic structure of the excitations. We hope that our work will stimulate interest in quantum statistical behaviour away from the low density limit. Indeed, because Bose condensates are stabilised by interactions, i.e. nonlinearities, it is necessary to go beyond the low-density, linear regime if a polariton condensate is ever to be observed. While the idea of a Bose condensate of cavity polaritons has been discussed for many years, this fact seems to have largely been overlooked; only very recently [37, 38] have bosonic effects been considered for interacting polaritons.

Experimental work has also concentrated on microcavities containing high-quality GaAs quantum wells. In these systems, the excitons

are weakly-bound, and rather delocalised. Thus, while the saturation nonlinearity discussed in this thesis is present for these excitations, it will be accompanied by other nonlinearities produced by the overlap of the wavefunctions of different excitons and the ionisation of excitons [10, 11]. These effects may well prevent condensation, but can be separated from the saturation nonlinearity of the present work by considering systems with localised, tightly-bound excitons. Note also that tightly-bound excitons have a large dipole coupling g, and hence the transition temperature will be larger.

For real examples of localised oscillators, there will be some energy E_m above which delocalised states exist. The picture of a condensate formed from localised oscillators then only holds when $E_m - \mu_{ex}$ is large compared with β^{-1} and g. By considering Fig. 4.1, we deduce that to completely realise a reentrant phase diagram like that shown in Fig. 3.1 requires an energy gap ΔE separating the localised excitations from the delocalised excitations; this gap must be large compared with g and β^{-1}. Such a gap could occur in organic semiconductors [15, 16]. In these systems, excitons are strongly bound and therefore small(Frenkel). They readily self-trap on local lattice distortions and on impurities in these, often highly disordered, materials. An energy gap ΔE could exist in inorganic quantum wells if the excitons move in a potential containing deep, well-separated traps, perhaps associated with interface islands in narrow quantum wells [19, 61, 62]. However, in both these examples it is likely that there will be several exciton states on each site, rather than a single state as we have assumed.

The disordered quantum wells studied by Hegarty et al. [21] provide an example of a system without a gap separating the localised from the delocalised excitations. These systems show a single inhomogeneously broadened exciton line, unlike the quantum wells mentioned above. The "mobility edge" E_m lies near to the centre of the exciton line. One may be able to form a condensate which does not involve delocalised excitations using this type of quantum well if the inhomogeneous broadening is large compared with g and β and the cavity mode is placed low down in the exciton line. The transition would then occur when the chemical potential is well separated from E_m.

The Dicke model (1.15) is one of the basic models of laser physics.

64

Similar two-level models have also been proposed to explain the coherent microwave emission from Josephson junction arrays [63]. Since the signature of a Bose condensate is coherence, and in a polariton condensate this coherence will appear in the photons, it is important to understand the distinction between lasing and polariton condensation. The distinction is that, unlike the laser, the polariton condensate has coherence in the electronic states [64]. As we have shown, the absorption spectrum in the condensed state of the model (1.19) has a gap. This gap is absent in a conventional laser, and so provides a clear experimental signature of polariton condensation.

5.1 FUTURE DIRECTIONS

5.1.1 RELATION TO LASERS

In a conventional laser, the gap in the absorption spectrum is destroyed because the polarisation in the gain medium is assumed to be very heavily damped [65]. We suggest that the relationship between polariton condensation and lasing should be explored by adding processes which damp the polarisation of the electronic states to the model (1.19). Such processes are analogous to the phase-breaking processes familiar in superconductors, which are usually associated with magnetic impurities [66, 67]. These impurities can actually produce a regime of gapless superconductivity, where there is an order parameter but no gap in the excitation spectrum. This suggests that the relationship between polariton condensation and lasing may be analogous to the relationship between normal and gapless superconductors.

5.1.2 NON-EQUILIBRIUM: FINITE LIFETIMES

More generally, we note that the most serious difficulty in making a polariton condensate experimentally is likely to be achieving thermal equilibrium before the excitation escapes from the cavity. To help to establish whether this is possible, we suggest that a non-equilibrium generalisation of the present theory should be constructed. Such a theory should be constructed by adding reservoirs [68] to the model (1.19), to represent, for example, the electromagnetic field outside the

cavity, and solving the dynamics of the model in the presence of these reservoirs. This theory could be used to explore the effects of finite lifetimes of the excitations on the polariton condensate.

While we leave a detailed investigation of whether the polariton condensate survives away from equilibrium for future work, we suggest one straightforward inequality which can be used to rule out the possibility of polariton condensation in some cases. The condensate has a natural energy scale $g|\lambda|$. A lifetime τ for the excitation corresponds to an energy h/τ. Thus we suggest that to realise the polariton condensate will require

$$g|\lambda| \gg h/\tau. \tag{5.1}$$

The lifetime of an excitation in the condensate, τ, is unknown. In principle it could be different from the lifetime of an excitation in the normal state, and should be calculated using the non-equilibrium theory. But it seems unlikely that it could exceed τ_c, the lifetime of the cavity mode produced by the finite reflectivity of the mirrors. Recall also that $|\lambda|^2$ is the number of photons per possible electronic excitation in the cavity, which must be less than $d = \rho_{ex} + 1/2$, the total number of excitations per possible electronic excitation. Using these two bounds in (5.1) we see that the condensate cannot exist unless

$$g\sqrt{d} \gg h/\tau_c. \tag{5.2}$$

5.1.3 NON-EQUILIBRIUM: COHERENT PUMPING

As well as coupling the model (1.19) to thermal reservoirs, it would be useful to develop a non-equilibrium theory which allowed for *coherent* external fields. Such a theory would permit the study of driven analogs [58, 64] of Bose condensation in microcavities [37, 38, 59]. In such analogs, the coherence does not appear spontaneously, but is, at least partly, inherited from an external pump. A theory of such driven condensates would also help to elucidate the connections between Bose condensation of polaritons and classical nonlinear optics [69].

5.1.4 Equilibrium Generalisations

Returning to the equilibrium condensate, there are several generalisations which would make the model (1.19) more realistic for particular systems. For high-quality quantum wells, one could incorporate direct interactions between excitons at a mean-field level [66]. For organics, and other materials with Frenkel excitons, one could allow for the possibility that there are several excitations on each site, rather than the single excitation of the model (1.19). Similar generalisations could also be made for disordered quantum wells; however, the structure of the electronic states in these systems is not yet fully understood, so quantitative generalisations are unlikely to be possible.

Finally, it would be interesting to study the model which corresponds to (1.19) with propagating photons which have a very small mass. We suspect that this problem could be solved by using the mass of the photons to construct a small parameter, and that this will give a mean-field theory identical to the one given in this thesis but controlled by the mass of the photon rather than $1/N$. This would provide a rigorous justification for our neglect of propagating photons in the model (1.19), even in a perfect, infinite planar cavity.

5.2 Concluding Summary

We have studied Bose condensation of cavity polaritons using the idealised model (1.19). Using a variational approach similar to the BCS theory of superconductivity, we have shown that the ground state of (1.19), in the presence of a chemical potential to constrain the polariton number, is a polariton condensate. This polariton condensate is a superposition of coherent photons and coherent electronic excitations, and is favoured over the normal state by the dipole interaction. We have shown

- How to generalise the concept of a polariton condensate from the low-density regime to include the fermionic structure of the electronic excitations.

- How to include an energy distribution for the electronic excitations in the description of the polariton condensate.

- That, in general, neither the fermionic structure nor the energy distribution of the electronic states precludes the existence of a polariton condensate.

We have also applied a path-integral technique to investigate the thermodynamics of the model (1.19), again using a chemical potential to produce a population of polaritons. The path-integral technique becomes *exact* in the limit $N \to \infty$; such exact solutions are rather unusual in models with local constraints like (1.18). The path-integral technique has shown

- That the variational approach was an exact description of the ground state when there are a large number of electronic oscillators in the cavity.

- That, at finite temperatures, there is a phase boundary separating the polariton condensate from an incoherent population of electronic excitations.

- That this phase boundary has unusual reentrant behaviour produced by the fermionic structure of the electronic excitations.

- That the scale of the critical temperature for condensation is set by the strength of the dipole interaction g.

- That the polariton condensate is constructed from a thermalised population of electronic excitations, renormalised by the electromagnetic field in the cavity.

Finally, by studying the excitation spectra, we have

- Explained the origin of the phase diagrams, and

- Shown that the absorption spectrum of the condensate has a gap, and could therefore be used to distinguish condensation from lasing.

Appendix A

THE GOLDSTONE MODE

IN THIS APPENDIX, we investigate the zero eigenvalue of $\mathcal{G}^{-1}$ that appeared while studying the stability of the condensate in the homogeneous case. We show that this zero is also present in the inhomogeneous model, and that it describes phase fluctuations of the condensate. It is thus the Goldstone mode reflecting the degeneracy of the ground state with respect to the phase of the order parameter. We then argue that this zero eigenvalue does not contribute to the free energy density in the thermodynamic limit. Although the physics we discuss in this appendix is well understood in general, it is particularly transparent in our simple model.

We note that, at $\omega = 0$, K_1 is real and positive. The eigenvalues of $\mathcal{G}^{-1}$ are then $K_1 \pm |K_2|$. Since from the explicit forms of K_1, K_2 and the extremal equation (3.4) we have $|K_2| = K_1$, as required in general by the Hugenholtz-Pines relation [49, 70], $\mathcal{G}^{-1}$ has a zero eigenvalue.

To illustrate that the zero eigenvalue is the phase mode of the condensate, note that since $\arg K_2 = 2 \arg \lambda = 2\phi$ we can write

$$
\mathcal{G}^{-1} \propto \begin{pmatrix} 1 & e^{2i\phi} \\ e^{-2i\phi} & 1 \end{pmatrix}.
$$

The eigenvector of this matrix with zero eigenvalue is perpendicular in the complex plane to the order parameter λ.

Since we are considering a broken symmetry system, we should not include states with different phases of the order parameter when cal-

culating the partition function. Thus on physical grounds, we should discard this zero mode when computing the partition function.

A formal approach which allows calculations in the presence of this zero eigenvalue is to introduce symmetry breaking terms which are taken to zero after the thermodynamic limit. This is the standard method for applying statistical mechanics to broken symmetry systems [50]. The appropriate symmetry breaking terms for a Bose condensed system pin the phase of the order parameter. They are sources and sinks for the photons, and appear in the effective action S_{eff} as $\frac{1}{\sqrt{N}} \left(\bar{\psi} J + \bar{J} \psi \right)$. These terms do not contribute directly to (3.10), but appear as a source term in (3.4). The original zero eigenvalue of $\mathcal{G}^{-1}$ is now $K_1 - |K_2| = -J/(\psi_0 \sqrt{N})$. Since for the equilibrium solution we must have $\phi - \arg J = \pi$, the contribution of the original zero eigenvalue to the free energy density is proportional to

$$\lim_{J \to 0} \lim_{N \to \infty} \frac{1}{N} \ln \left(\frac{|J|}{|\lambda| \sqrt{N}} \right) = 0.$$

70

Bibliography

[1] J. J. Hopfield, "Theory of the Contribution of Excitons to the Complex Dielectric Constant of Crystals", *Phys. Rev.* **112**(5), 1555 (1958).

[2] C. Klingshirn, *Semiconductor Optics*, Springer, Berlin, 1997.

[3] C. Kittel, *Quantum Theory of Solids*, John Wiley and Sons, New York, 1963.

[4] E. Hanamura and H. Haug, "Condensation Effects of Excitons", *Physics Reports* **33**(4), 209–284 (1977).

[5] H. Haug and S. Koch, *Quantum Theory of the Optical and Electronic Properties of Semiconductors*, World Scientific, 1990.

[6] C. Weisbuch, M. Nishioka, A.Ishikawa, and Y.Arakawa, "Observation of the Coupled Exciton-Photon Mode Splitting in a Semiconductor Quantum Microcavity", *Phys. Rev. Lett.* **69**(23), 3314–3317 (1992).

[7] M. S. Skolnick, T. A. Fisher, and D. M. Whittaker, "Strong Coupling Phenomena in Quantum Microcavity Structures", *Semicond. Sci. Technol.* **13**, 645–669 (1998).

[8] F. Jahnke, M. Kira, and S. W. Koch, "Theory of Nonlinear Exciton Saturation in Semiconductor Microcavities", *Phys. Stat. Sol.* **206**, 19–25 (1998).

[9] S. Schmitt-Rink, D. S. Chemla, and D. A. B. Miller, "Theory of Transient Excitonic Optical Nonlinearities in Semiconductor Quantum-Well Structures", *Phys. Rev. B* **32**(10), 6601–6609 (1985).

[10] R. Houdré, J. L. Gibernon, P. Pellandini, R. P. Stanley, U. Oesterle, C. Weisbuch, J. O'Gorman, B. Roycroft, and M. Ilegems, "Saturation of the Strong-coupling Regime in a Semiconductor Microcavity: Free-carrier Bleaching of Cavity Polaritons", *Phys. Rev. B* **52**(11), 7810–7813 (1995).

[11] F. Jahnke, M. Kira, S. W. Koch, G. Khitrova, E. K. Lindmark, T. R. Nelson, Jr, D. V. Wick, J. D. Berger, O. Lyngnes, H. M. Gibbs, and K. Tai, "Excitonic Nonlinearities of Semiconductor Microcavities in the Nonperturbative Regime", *Phys. Rev. Lett.* **77**(26), 5257–5260 (1996).

[12] A. I. Tartakovskii, V. D. Kulakovskii, Y. I. Koval', T. B. Borzenko, A. Forchel, and J. P. Reithmaier, "Exciton-Photon Interaction in Low-Dimensional Semiconductor Microcavities", *JETP* **87**(4), 723–730 (1998).

[13] J. Bloch, F. Bœuf, J. M. Gérard, B. Legrand, J. Y. Marzin, R. Planel, V. Thierry-Mieg, and E. Costard, "Strong and Weak Coupling Regime in Pillar Semiconductor Microcavities", *Physica E* **2**(1–4), 915–919 (1998).

[14] T. Gutbrod, M. Bayer, A. Forchel, J. P. Reithmaier, T. L. Reinecke, S. Rudin, and P. A. Knipp, "Weak and Strong Coupling of Photons and Excitons in Photonic Dots", *Phys. Rev. B* **57**(16), 9950–9956 (1998).

[15] D. G. Lidzey, D. D. C. Bradley, M. S. Skolnick, T. Virgili, S. Walker, and D. M. Whittaker, "Strong Exciton-Photon Coupling in an Organic Semiconductor Microcavity", *Nature* **395**(3), 53–55 (1998).

[16] D. G. Lidzey, D. D. C. Bradley, T. Virgili, A. Armitage, M. S. Skolnick, and S. Walker, "Room Temperature Polariton Emission from Strongly Coupled Organic Semiconductor Microcavities", *Phys. Rev. Lett.* **82**(16), 3316–3319 (1999).

[17] A. Tredicucci, Y. Chen, V. Pelligrini, M. Börger, L. Sorba, F. Beltram, and F. Bassani, "Controlled Exciton-Photon Interaction

72

in Semiconductor Bulk Microcavities", *Phys. Rev. Lett.* **75**(21), 3906–3909 (1995).

[18] P. Kelkar, V. Kozlov, H. Jeon, A. V. Nurmikko, C.-C. Chu, D. C. Grillo, J. Han, C. G. Hua, and R. L. Gunshor, "Excitons in a II-VI Semiconductor Microcavity in the Strong-Coupling Regime", *Phys. Rev. B* **52**(8), R5491–R5494 (1995).

[19] H. F. Hess, E. Betzig, T. D. Harris, L. N. Pfeiffer, and K. W. West, "Near-Field Spectroscopy of the Quantum Constituents of a Luminescent System", *Science* **264**, 1740–1745 (1994).

[20] J. Hegarty, M. D. Sturge, C. Weisbuch, A. C. Gossard, and W. Wiegmann, "Resonant Rayleigh Scattering from an Inhomogeneously Broadened Transition: A New Probe of the Homogeneous Linewidth", *Phys. Rev. Lett.* **49**(13), 930–932 (1982).

[21] J. Hegarty, L. Goldner, and M. D. Sturge, "Localized and Delocalized Two-Dimensional Excitons in GaAs-AlGaAs Multiple-quantum-well Structures", *Phys. Rev. Lett.* **30**(12), 7346–7348 (1984).

[22] D. Gammon, B. V. Shanabrook, and D. S. Katzer, "Exciton, Phonons, and Interfaces in GaAs/AlAs Quantum-Well Structures", *Phys. Rev. Lett.* **67**(12), 1547–1550 (1991).

[23] N. Garro, L. Pugh, R. T. Phillips, V. Drouot, M. Y. Simmons, B. Kardynal, and D. A. Ritchie, "Resonant Rayleigh Scattering by Excitonic States Laterally Confined in the Interface Roughness of $GaAs/Al_xGa_{1-x}As$ Single Quantum Wells", *Phys. Rev. B* **55**(20), 13752–13760 (1997).

[24] V. Savona, S. Haacke, and B. Deveaud, "Optical Signatures of Energy-Level Statistics in a Disordered Quantum System", *Phys. Rev. Lett.* **84**(1), 183–186 (2000).

[25] M. G. Raizen, R. J. Thompson, R. J. Breccha, H. J. Kimble, and H. J. Carmichael, "Normal-Mode Splitting and Linewidth Averaging for Two-State Atoms in an Optical Cavity", *Phys. Rev. Lett.* **63**(3), 240–243 (1989).

73

[26] R. H. Dicke, "Coherence in Spontaneous Radiation Processes", *Phys. Rev.* **93**, 99–110 (1954).

[27] L. Allen and J. H. Eberly, *Optical Resonance and Two-level Atoms*, Dover, New York, 1975.

[28] A. Auerbach, *Interacting Electrons and Quantum Magnetism*, Springer, New York, 1994.

[29] R. Houdré, R. P. Stanley, and M. Ilegems, "Vacuum-field Rabi Splitting in the Presence of Inhomogeneous Broadening: Resolution of a Homogeneous Linewidth in an Inhomogeneously Broadened System", *Phys. Rev. A* **53**(4), 2711–2715 (1996).

[30] C. Ell, J. Prineas, T. R. Nelson, S. Park, H. M. Gibbs, G. Khitrova, S. W. Koch, and R. Houdré, "Influence of Structural Disorder and Light Coupling on the Excitonic Response of Semiconductor Microcavities", *Phys. Rev. Lett.* **80**(21), 4795–4798 (1998).

[31] D. M. Whittaker, "What Determines Inhomogeneous Linewidths in Semiconductor Microcavities?", *Phys. Rev. Lett.* **80**(21), 4791–4794 (1998).

[32] D. S. Citrin, "Radiative Lifetimes of Excitons in Quantum Wells: Localisation and Phase-coherence Effects", *Phys. Rev. B* **47**(7), 3832–3841 (1993).

[33] D. A. Eastham, *Atomic Physics of Lasers*, Taylor and Francis, London, 1986.

[34] P. Senellart and J. Bloch, "Nonlinear Emmission of Microcavity Polaritons in the Low Density Regime", *Phys. Rev. Lett.* **82**(6), 1233–1236 (1999).

[35] L. S. Dang, D. Heger, R. André, F. Bœuf, and R. Romestain, "Stimulation of Polariton Photoluminescence in Semiconductor Microcavity", *Phys. Rev. Lett.* **81**(18), 3920–3923 (1998).

[36] V. Pellegrini, R. Colombelli, L. Sorba, and F. Beltram, "Acoustic-phonon-mediated Polariton Photoluminescence in a GaAs Bulk Microcavity", *Phys. Rev. B* **59**(15), 10059–10063 (1999).

[37] P. G. Savvidis, J. J. Baumberg, R. M. Stevenson, M. S. Skolnick, D. M. Whittaker, and J. S. Roberts, "Angle-resonant Stimulated Polariton Amplifier", *Phys. Rev. Lett.* **84**(7), 1547–1550 (2000).

[38] R. M. Stevenson, V. N. Astratov, M. S. Skolnick, D. M. Whittaker, E. Emam-Ismail, A. I. Tartakovskii, P. G. Savvidis, J. J. Baumberg, and J. S. Roberts, "Continuous Wave Observation of Massive Polariton Redistribution by Stimulated Scattering in Semiconductor Microcavities", *Phys. Rev. Lett.* **85**(17), 3680–3683 (2000).

[39] A. Griffin, D. W. Snoke, and S. Stringari, editors, *Bose-Einstein Condensation*, Cambridge University Press, Cambridge, U.K., 1995.

[40] A. J. Leggett, "Broken Gauge Symmetry in a Bose Condensate", in *Bose-Einstein Condensation*, edited by A. Griffin, D. W. Snoke, and A. Stringari, pages 452–462, Cambridge University Press, Cambridge, U.K., 1995.

[41] P. Nozières, "Some Comments on Bose-Einstein Condensation", in *Bose-Einstein Condensation*, edited by A. Griffin, D. W. Snoke, and A. Stringari, pages 15–30, Cambridge University Press, Cambridge, U.K., 1995.

[42] P. Nozières and D. S. James, "Particle vs. Pair Condensation in Attractive Bose Liquids", *J. Phys. (Paris)* **43**, 1133–1148 (1982).

[43] N. K. Wilkin, J. M. F. Gunn, and R. A. Smith, "Do Attractive Bosons Condense?", *Phys. Rev. Lett.* **80**(11), 2265–2268 (1998).

[44] K. Hepp and E. H. Lieb, "On the Superradiant Phase Transition for Molecules in a Quantized Radiation Field: the Dicke Maser Model", *Ann. Phys.* **76**, 360–404 (1973).

[45] V. F. Elesin and Y. V. Kopaev, "Contribution to the Electron Theory of Ferroelectricity", *Pism'a Zh. Eksp. Teor. Fiz.* **24**(2), 78–81 (1976), [JETP Lett. **24**(2), 66–69].

[46] C. Comte and P. Nozières, "Exciton Bose Condensation: The Ground State of an Electron-Hole Gas. I: Mean Field Description of a Simplified Model", *Journal de Physique* **43**, 1069–1081 (1982).

[47] B. D. Simons, "Concepts in Theoretical Physics", Notes on Lectures given at Cambridge University, presently available from http://www.tcm.phy.cam.ac.uk/~bds10/.

[48] L. S. Schulman, *Techniques and Applications of Path Integration*, John Wiley and Sons, Inc., New York, 1981.

[49] V. N. Popov and V. S. Yarunin, *Collective Effects in Quantum Statistics of Radiation and Matter*, Kluwer Academic Publishers, Dordrecht, 1988.

[50] J. W. Negele and H. Orland, *Quantum Many-Particle Systems*, Addison-Wesley, Redwood City, California, 1988.

[51] V. B. Kir'yanov and V. S. Yarunin, "Superradiance for Lattice Model with Lee Interaction", *Toer. Matematicheskaya Fiz.* **43**(1), 91–99 (1980), [Theoretical and Mathematical Physics **43**(1), 340–345].

[52] G. B. Arfken and H. J. Weber, *Mathematical Methods for Physicists*, Academic Press, 1995.

[53] V. M. Galitskii, S. P. Goreslavskii, and V. F. Elesin, "Electric and Magnetic Properties of a Semiconductor in the Field of a Strong Electromagnetic Wave", *Zh. Eksp. Teor. Fiz.* **30**(1), 207–217 (1969), [Sov. Phys. JETP **30**(1), 117–122].

[54] K. Rzążewski, K. Wódkiewicz, and W. Żakowicz, "Remark on the Superradiant Phase Transition", *Phys. Lett.* **58A**(4), 211–212 (1976).

[55] K. Rzążewski, K. Wódkiewicz, and W. Żakowicz, "Phase Transitions, Two-Level Atoms, and the A^2 Term", *Phys. Rev. Lett.* **35**(7), 432–434 (1975).

[56] D. Forster, *Hydrodynamic Fluctuations, Broken Symmetry and Correlation Functions*, Number 47 in Frontiers in Physics, W. A. Benjamin, Inc., Reading, Massachusetts, 1975.

[57] P. B. Littlewood and C. M. Varma, "Amplitude Collective Modes in Superconductors and their Coupling to Charge-density Waves", *Phys. Rev. B* **26**(9), 4883–4893 (1982).

[58] S. Schmitt-Rink, D. S. Chemla, and H. Haug, "Nonequilibrium Theory of the Optical Stark Effect and Spectral Hole Burning in Semiconductors", *Phys. Rev. B* **37**(2), 941–955 (1988).

[59] F. Quochi, G. Bongiovanni, A. Mura, J. L. Staehli, B. Deveaud, R. P. Stanley, U. Oesterle, and R. Houdrè, "Strongly Driven Semiconductor Microcavities: From the Polariton Doublet to an ac Stark Triplet", *Phys. Rev. Lett.* **80**(21), 4733–4736 (1998).

[60] H. Cao, S. Pau, J. M. Jaobson, G. Björk, Y. Yamamoto, and A. Imamoğlu, "Transition from a Microcavity Exciton Polariton to a Photon Laser", *Phys. Rev. A* **55**(6), 4632–4635 (1997).

[61] D. Gammon, E. S. Snow, B. V. Shanabrook, D. S. Katzer, and D. Park, "Fine Structure Splitting in the Optical Spectra of Single GaAs Quantum Dots", *Phys. Rev. Lett.* **76**(16), 3005–3008 (1996).

[62] N. H. Bonadeo, G. Chen, D. Gammon, D. S. Katzer, D. Park, and D. G. Steel, "Nonlinear Nano-Optics: Probing One Exciton at a Time", *Phys. Rev. Lett.* **81**(13), 2759–2762 (1998).

[63] P. Barbara, A. B. Cawthorne, S. V. Shitov, and C. J. Lobb, "Stimulated Emission and Amplification in Josephson Junction Arrays", *Phys. Rev. Lett.* **82**(9), 1963–1966 (2000).

[64] S. A. Moskalenko and D. W. Snoke, *Bose-Einstein Condensation of Excitons and Biexcitons*, CUP, Cambridge, U.K., 2000.

77

[65] H. Haken, "Cooperative Phenomena in Systems Far From Thermal Equilibrium and in Nonphysical Systems", *Rev. Mod. Phys.* **47**, 67 (1975).

[66] P. B. Littlewood and P. Eastham, Exciton Condensation, in *Optical Properties of Semiconductor Nanostructures*, edited by M. L. Sadowski, M. Potemski, and M. Grynberg, volume 81 of *NATO Science High Technology*, pages 133–141, Dordrecht, The Netherlands, 2000, Kluwer.

[67] K. Maki, "Gapless Superconductivity", in *Superconductivity*, edited by R. D. Parks, volume 2, chapter 18, pages 1035–1105, Marcel Dekker, Inc., New York, 1969.

[68] A. O. Caldeira and A. J. Leggett, "Influence of Dissipation on Quantum Tunnelling in Macroscopic Systems", *Phys. Rev. Lett.* **46**(4), 211–214 (1981).

[69] L. V. Keldysh, "Macroscopic Coherent States of Excitons in Semiconductors", in *Bose-Einstein Condensation*, edited by A. Griffin, D. W. Snoke, and A. Stringari, Cambridge University Press, Cambridge, U.K., 1995.

[70] N. M. Hugenholtz and D. Pines, "Ground-state Energy and Excitation Spectrum of a System of Interacting Bosons", *Phys. Rev.* **116**(3), 489–506 (1959).